Cement and Concrete Research 209 (2026) 108373

Contents lists available at ScienceDirect

Cement and Concrete Research

journal homepage: www.elsevier.com/locate/cemconres

Chloride binding isotherms for Alkali-Activated Slag systems — Pitfalls in the equilibrium method and data interpretation

Annika Lidwina Schultheiß [a,*], Klaartje de Weerdt [b], Natalia Palina [c], Mayank Gupta [a], Barbara Lothenbach [b], Ravi A. Patel [a], Frank Dehn [a]

[a] Institute of Building Materials and Concrete Structures (IMB), Karlsruhe Institute of Technology, Kaiserstr. 12, Karlsruhe, 76131, Germany
[b] Department of Structural Engineering, Norwegian University of Science and Technology, Richard Birkelands vei 1 A, Trondheim, 7034, Norway
[c] Institute for Nuclear Waste Disposal (INE), Karlsruhe Institute of Technology, Kaiserstr. 12, Karlsruhe, 76131, Germany

ARTICLE INFO

Keywords:
Chloride binding isotherms
Alkali-activated slag systems
Equilibrium method
Microstructural quantification
Thermodynamic simulation

ABSTRACT

Determining chloride binding isotherms through equilibrium experiments is common practice in studies on cementitious materials. However, inaccuracies and inconsistencies in experimental procedures and evaluation methods result in non-comparable isotherms. This study critically evaluates the *equilibrium method* and its interpretation for determining chloride binding isotherms. By comparing the *equilibrium method* for Ordinary Portland cement (OPC) paste with two alkali-activated slag (AAS) pastes, inaccuracies that originate from different experimental evaluation protocols are evaluated. Microstructural evidence from TGA, XRD and SEM–EDS in combination with thermodynamic modelling is used to further investigate processes affecting the measurement of the chloride binding capacity of alternative binders.

It was found that the simplification of neglecting the initial water content of the paste causes a *diluting effect* that lowers the measured equilibrium chloride concentration and leads to an overestimation of the bound chloride content. It is also demonstrated that, especially for AAS pastes, water-binding reactions during equilibration can cause a reduction in liquid volume, which increases the measured equilibrium chloride concentration. This *volume effect* leads to an underestimation of the chloride binding capacity of AAS paste. A key novelty of this study is the quantitative correction of this error by measuring the chemically bound water content before and after chloride exposure. Overall, this study highlights critical methodological pitfalls and provide clear guidelines for determination of chloride binding isotherms using the *equilibrium method*.

1. Introduction

Chloride ingress is widely recognized as one of the most critical durability challenges for reinforced concrete structures [1]. As chlorides accumulate at the steel surface, they can depassivate the reinforcement, triggering corrosion and thus significantly reducing service life. To meet increasing sustainability demands, alternative binder systems with reduced clinker content are being developed. Among them, alkali-activated slag (AAS) has emerged as a promising option due to favourable mechanical [2,3] and durability-related properties [4–6]. However, AAS differs substantially from conventional Portland cement-based binders defined in EN 197-1 [7] and therefore long-established durability design approaches may not be directly transferable. Therefore, a more mechanistic understanding of the chloride resistance of AAS systems is needed. For this, both the effective diffusion coefficient [8] and the chloride binding capacity [9] must be analysed, since these properties are strongly influenced by the chemical composition of the binder, and the reaction products and microstructure of the paste. Currently, no reliable prediction of the chloride binding capacity of concrete is available [10,11] (see Appendix A.1). Consequently, the accurate experimental determination of the chloride binding capacity is essential for understanding the durability of AAS and other emerging binder systems.

Two main mechanisms of chloride binding are commonly distinguished in the literature: chemical and physical binding. Chemical binding refers to the incorporation of chloride ions into the crystal structure of solid phases. In traditional OPC-based systems, this mechanism is mainly associated with the formation of chloride-containing AFm phases such as Friedel's and Kuzel's salts [12], and hydrotalcite-like phases [13]. Physical binding, in contrast, corresponds to the adsorption of chloride ions onto the surface of solid phases, with calcium-silicate-hydrate (C–S–H) phase being the principal contributor [14].

* Corresponding author.
E-mail address: annika.schultheiss@kit.edu (A.L. Schultheiß).

https://doi.org/10.1016/j.cemconres.2026.108373
Received 8 April 2026; Received in revised form 5 August 2026; Accepted 11 August 2026
Available online 27 August 2026

For AAS pastes, only (limited) formation of Friedel's salt has been reported [15,16]. Several studies [16,17] indicate that AAS generally does not form sulphate-bearing AFt or sulphate-bearing AFm phases, which in OPC systems chemically bind chlorides in the form of Kuzel's salt. Instead, AAS may develop strätlingite (an AFm-like phase), which has been shown to bind chlorides weakly and in a pH-sensitive manner through a hydrocalumite-like structure [16,18,19]. Chloride binding in AAS can also occur through hydrotalcite [16–19], which is a Layered Double Hydroxide (LDH). However, hydrotalcite typically represents only a minor crystalline fraction. Physical binding due to adsorption of chloride on calcium alkali aluminosilicate hydrate (C–(N)–(A)–S–H) phases is a major component of the chloride binding capacity of AAS pastes [15–17], although its binding capacity is lower compared to LDHs [20].

The chloride binding capacity of paste is commonly expressed through chloride binding isotherms. Chloride binding isotherms describe the relationship between the bound chlorides in the paste $C_{Cl,b}$ [g Cl/g dry paste] and the equilibrium concentration of free chlorides in the liquid $C_{Cl,eq}$, usually expressed in [mol Cl/l liquid]. The bound chloride concentration $C_{Cl,b}$ may also be expressed in units of [g Cl/g cement] [21–23] to enable better comparability with total chloride contents obtained from chloride profiles, which are commonly reported in the same unit. However, converting from paste mass to cement mass can be done either using the water-to-binder ratio from the mix design [21,23] or the measured chemically bound water content [22], and these different approaches may introduce inconsistencies in the reported values. Based on experimental data from multiple equilibrium samples linear isotherms (Eq. (1)), Freundlich isotherms (Eq. (2)), or Langmuir isotherms (Eq. (3)) can be fitted. However, when the relationships described in Eqs. (1)–(3) are fitted using free chloride concentrations measured before the equilibrium is reached, as reported in several studies (e.g. [11,13,23–25]), the resulting curves cannot be considered valid chloride binding isotherms, because the free chloride concentration at equilibrium is needed.

$$C_{Cl,b} = m \cdot C_{Cl,eq} \tag{1}$$

were m is constant.

$$C_{Cl,b} = k \cdot C_{Cl,eq}^{n} \tag{2}$$

were k and n are constants.

$$C_{Cl,b} = \frac{a \cdot C_{Cl,eq}}{1 + b \cdot C_{Cl,eq}} \tag{3}$$

were a and b are constants.

Methods to investigate the chloride binding capacity of cementitious binders with SCMs are reviewed by the *RILEM TC 298-EBD* [9]. They highlight the gaps limiting the comparison between experimental studies due to the lack of a standard protocol. They identify the *equilibrium method* as a simple experimental concept to measure the chloride binding isotherm, where paste is exposed to a known chloride concentration and the chloride binding capacity is measured once equilibrium is reached. Differences in the experimental protocol discussed by the *RILEM TC 298-EBD* are (1) the use of crushed material or paste discs, (2) the direct investigation of chloride binding capacity of the solid or, the indirect investigation of the liquid phase, (3) the solid to liquid ratio and, (4) the type of exposure solution. The standard test setup of the *equilibrium method* is using crushed samples and the indirect investigation, which is applied to pastes made of OPC (e.g. [11,13,21,22,26–31]), blended binders with SCMs (e.g. [10,23,31–33]) and alkali-activated binders (e.g. [15,19,24,25,34,35]). The detailed review of these studies (summarized in Appendix A.2) revealed additional differences in the experimental procedure and evaluation protocols, which influence the reported binding capacity. In general, the amount of bound chlorides ($C_{Cl,b}$ [g Cl/g dry paste]) at equilibrium is indirectly determined by the concentration of the free chloride in the liquid as:

$$C_{Cl,b} = \frac{M_{Cl} \cdot \left(n_{Cl,init} - n_{Cl,eq}\right)}{m_{sample,dry}} \tag{4}$$

where M_{Cl} = 35.45 g/mol is the molar mass of chloride, $n_{Cl,init}$ and $n_{Cl,eq}$ [mol] are the amounts of chloride in the initial and equilibrium solutions, and $m_{sample,dry}$ [g] is the mass of the dry paste.

In most experimental procedures, moisture-containing paste is added into the chloride-bearing solution. This addition inevitably dilutes the added chloride concentration ($C_{Cl,added}$) due to the initial pore water contained in the paste ($m_{pore,0}$). The effect becomes increasingly significant at higher solid-to-liquid ratios. Therefore, initial chloride concentration ($C_{Cl,init}$ [mol/l]) must be calculated as follows:

$$C_{Cl,init} = \frac{C_{Cl,added} \cdot V_{added}}{V_{added} + V_{pore,0}} \tag{5}$$

where $C_{Cl,added}$ [mol/l] is chloride concentration in added solution, V_{added} [m^3] is the volume of the added solution and $V_{pore,0}$ is the volume of the free water content in the paste before exposure. Assuming the density of water being 1 g/cm^3, $V_{pore,0}$ can be calculated based on the experimentally determined mass of initial pore water in the paste ($m_{pore,0}$).

Many studies (e.g. [13,22,23,30,31]) explicitly account for the free water content of the paste prior to exposure by adapting Eq. (4) as follows:

$$C_{Cl,b} = \frac{M_{Cl} \cdot \left(C_{Cl,init} - C_{Cl,eq}\right) \cdot V_{init}/1000}{m_{sample,0} - m_{pore,0}} \tag{6}$$

where $C_{Cl,eq}$ [mol/l] is the chloride concentration in the equilibrium solution, $V_{init} = V_{pore,0} + V_{added}$ [m^3] is the initial water content and, $m_{sample,0}$ is the mass of the moist paste.

Alternatively, some studies (e.g. in [24,25]) dry their sample completely before exposure. Assuming $m_{pore,0} == 0$, Eq. (6) can be simplified as follows:

$$C_{Cl,b} = \frac{M_{Cl} \cdot \left(C_{Cl,added} - C_{Cl,eq}\right) \cdot V_{added}/1000}{m_{sample,dry}} \tag{7}$$

However, drying of paste without changing the phase composition is a challenge. Prolonged drying even below 105 °C removes partially the chemically bound water of C–S–H, ettringite and monosulfate [36]. If samples are dried with liquid nitrogen combined with subsequent freeze–drying, ettringite, C–S–H and to a lesser extent monosulfate decompose, as they also lose a part of the water [36]. In contrast, short-term drying is not sufficient to remove all free water and need therefore to be combined with solvent exchange [36], which also alters the chemically bound water content in C–S–H, ettringite and monosulfate. In conclusion, the phase composition of dried samples is significantly different, therefore drying before exposure is not recommended to determine chloride binding isotherms for paste.

The most widely used *equilibrium method* was established by Tang and Nilsson [26], where the paste is dried at 11% relative humidity (RH) before exposure. They assumed that $C_{Cl,init}$ equals $C_{Cl,added}$, reasoning that after seven days of storage at 11% RH, the OPC paste would retain only a monolayer of water adsorbed on the gel surface. Consequently, they apply the simplification given in Eq. (7). The reference mass in Tang and Nilsson's study [26] however is not clearly described. We interpret that either the mass of the paste stored at 11% RH ($m_{sample,dry} = m_{sample,11RH}$) or the mass of the sample after drying at 105 °C ($m_{sample,dry} = m_{sample,105°C}$) can be used.

Several subsequent studies on OPC pastes [11,15,27,28,32] and AAS pastes [15] adopted a similar drying procedure at 11% RH. In OPC-based systems drying at 11% RH can be more effective than removing water by solvent-exchange [37]. However, AAS pastes possess a finer pore size distribution than OPC pastes [38] and, as predicted by the Kelvin equation [39], can therefore retain a higher amount of water at the same relative humidity. Thus, the assumption that $C_{Cl,init}$ equals $C_{Cl,added}$ may not be applicable to AAS pastes. To (maybe) correct for this, Zhang et al. [15] subtracted the initial water content ($m_{pore,0}$) remaining at 11% RH in the AAS paste from the dry mass at 11% RH ($m_{sample,11RH}$).

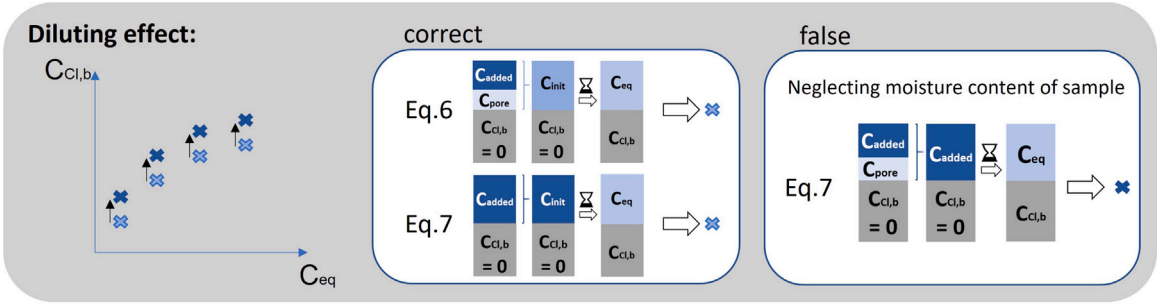

Fig. 1. Illustration of *diluting effect* on reported chloride binding isotherms.

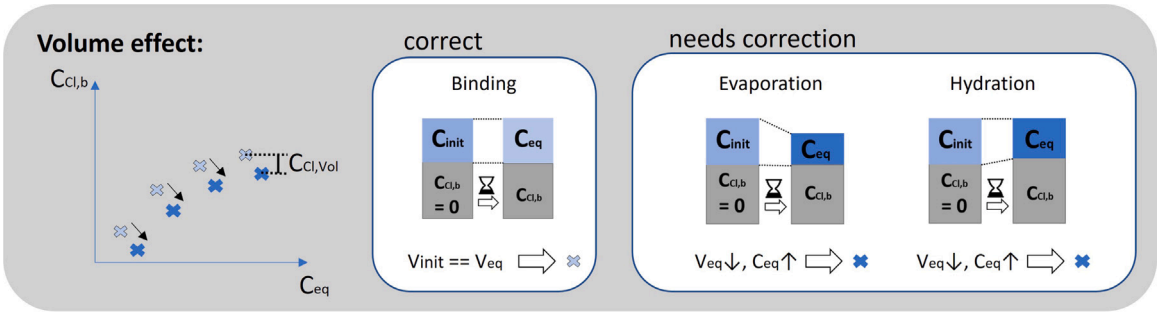

Fig. 2. Illustration of *volume effect* on reported chloride binding isotherms.

Other works [19,21,33,35] applied Eq. (7) without (proper) drying of the paste, which introduces methodological inconsistencies and limits the reliability and comparability of their data. The neglect of the initial moisture content results to a higher reference mass, which reduces the calculated bound chloride content. But the neglect of the initial moisture content also implies a higher starting concentration ($C_{Cl,added} > C_{Cl,init}$), which leads to a greater reduction in the chloride concentration in the pore solution and consequently an increase of the calculated bound chloride content. Overall, this *dilution effect* results in an overestimation of the bound chloride content ($C_{Cl,b}$) since the simplified formulation given in Eq. (7) predicts a higher bound chloride content than Eq. (6) whenever $C_{eq} < C_{added}$ and $m_{pore,0} > 0$. This *diluting effect* is illustrated in Fig. 1.

Furthermore, it should be emphasized that the indirect determination of chloride binding capacity, as described in Eqs. (6) and (7) relies on the (strong) assumption that the volume of liquid remains constant throughout the experiment. If this assumption is not fulfilled, the *volume effect* occurs, which is illustrated in Fig. 2. Here, the volume of liquid decreases during the experiment, which leads to an increase in the measured chloride concentration at equilibrium ($C_{Cl,eq}$), which can falsely be interpreted as a decrease in bound chloride content ($C_{Cl,b}$).

The resulting error in the chloride binding ($C_{Cl,Vol}$ [$g_{Cl}/g_{dry\ paste}$]), caused by changes in the liquid content of the equilibrium sample, can be calculated as follows:

$$C_{Cl,Vol} = \frac{M_{Cl} \cdot C_{Cl,eq} \cdot (V_{init} - V_{eq})/1000}{m_{sample,0} - m_{pore,0}} \quad (8)$$

where V_{eq} [m^3] is the volume of the liquid in sample after equilibrium is reached. Ipavec et al. [33] accounted for liquid loss during equilibration by monitoring the weight change of the total mass (container + paste + liquid) throughout the experiment. However, any mass loss due to evaporation should be strictly prevented, as it compromises the reproducibility and reliability of the experimental conditions. Another possible reason for the reduction in liquid volume is ongoing hydration, which chemically binds water. Therefore, several studies on OPC [13,22,23,30,31] introduced an additional curing step in which 30–40 w.% water was added to crushed paste to form "moist sand", which was then stored to maximize hydration before chloride exposure. However, such procedure cannot be applied to alternative binders such as AAS pastes, because the immersion to water can lead to leaching of the alkalis from the pore network of the material, hindering or halting strength and microstructural development upon immersion [40].

This review of the existing literature on chloride binding reveals substantial differences in both the experimental procedures and the evaluation protocols used to quantify chloride binding. The main variations in the evaluation protocols are related to whether the initial water content of the paste is taken into account and whether the reference mass is defined as the mass of the moist or the dry sample. OPC binding isotherms determined with different experimental procedures are illustrated in Fig. 3(a). It should be noted that the testing conditions used to determine chloride-binding isotherms, particularly the composition of the NaCl exposure solution, vary between studies. Nevertheless, a consistent trend can be observed: isotherms calculated based on the added chloride concentration (Eq. (7)) generally indicate a slightly higher binding capacity than those determined using the initial chloride concentration (Eq. (6)). This indicates the *diluting effect* due to the initial water content of the paste. If the reference mass is moist sample mass instead of the usually used dry reference mass, the calculated bound chloride content is lower. In Fig. 3(b), all available studies on AAS pastes [15,19,24,25,35] use $C_{Cl,added}$ for calculating the bound chloride content. Since AAS pastes generally exhibit a lower chemical chloride binding capacity, the *diluting effect* and a possible *volume effect* are expected to have a stronger influence on the calculated binding capacity. This raises the question if the reported high chloride binding capacities of AAS illustrated in Fig. 3(b) may be systematically overestimated.

In this study, a series of *equilibrium method* experiments were performed on AAS pastes, alongside OPC as a reference system. To quantify how the chosen evaluation protocol influences the estimated chloride binding, we compare chloride-binding isotherms calculated using Eqs. (6) and (7), thereby explicitly evaluating the effect of accounting for (or neglecting) the initial water content of the paste. Furthermore, we present the first application of Eq. (8) to account for the reduction in exposure solution volume due to water-binding reactions. While dilution and volume effects have been recognized and discussed for

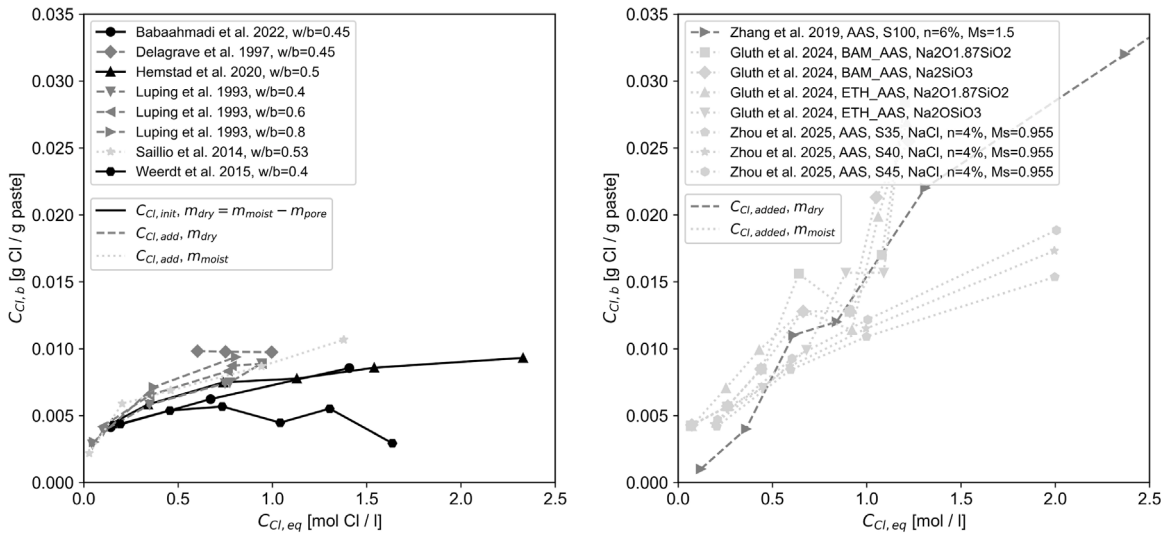

(a) OPC (b) AAS

Fig. 3. Comparison of (a) isotherms from OPC pastes [21,26,28–31] and, (b) isotherms from AAS pastes [15,19,35] determined with different evaluation protocols.

OPC systems, their systematic omission in AAS research presents a critical gap. Demonstrating and quantifying these effects for AAS systems, where high reactivity amplifies reaction-driven volume changes — constitutes a major novelty of this work and reveals that current practice (relying solely on Eq. (7)) can significantly distort the calculated binding capacity. To validate these indirectly derived binding capacities, the chloride binding phases in AAS paste are directly investigated using TGA and XRD. An in-depth SEM–EDS investigation provides, for the first time, a direct estimate of the chloride incorporation in the amorphous phases (C–N–A–S–H and hydrotalcite) of AAS systems. Thermodynamic modelling is further employed to contextualize and interpret the experimental findings. The overall objective of this work is to critically reassess the *equilibrium method* for AAS systems, including the evaluation protocols used to derive chloride binding isotherms, with the aim of improving the comparability across studies and identifying methodological pitfalls that currently hinder reliable interpretation of chloride binding in AAS systems.

2. Methods

2.1. Materials and sample preparation

The present study investigates two mixes composed of alkali-activated ground-granulated blast-furnace slag (GGBFS) and one mix with Ordinary Portland cement (OPC, CEM I 42.5) as a reference binder. Both investigated AAS pastes demonstrated our in previous studies favourable properties with respect to workability and mechanical performance when used in concrete [5,41]. Also, their microstructural development [42], reaction kinetics [43], and susceptibility to alkali–silica reaction [5] have been systematically characterized. The investigation of their chloride binding capacity thus, adds to the holistic analysis of these alternative binders. At the same time, potential methodological limitations of the established *equilibrium method*, when applied to alternative binders, can be assessed through a direct comparison with OPC paste.

The chemical compositions of GGBFS and OPC, along with the mix design of the pastes, are detailed in Tables 1 and 2. For the activation of the GGBFS, two different alkaline solutions were utilized, each with a sodium oxide content of $n = 4.0$ [g/100 g GGBFS]. They differ in the silica modulus ($M_S = SiO_2/Na_2O$ [mol/mol]) values with $M_S = 0.5$ and $M_S = 1.9$ for mixes AAS0.5 and AAS1.9, respectively. The alkaline solutions were prepared by mixing sodium hydroxide NaOH, waterglass, and distilled water. The NaOH solution had a solute mass concentration of 50%, while the waterglass used was Betol39T with a solute concentration of 34.5% and a molar ratio of $M_S = 3.4$ [mol/mol]. The chemical composition of both activator solutions is given in Appendix A.3. Both solutions were cooled to room temperature for 24 h before being mixed with GGBFS to reach temperature equilibrium with the surrounding environment (20 °C) [5,44]. The water to binder ratio for all pastes was 0.47.

To produce AAS paste, GGBFS was mixed with the alkaline solution using a high-shear mixer. The AAS paste was filled into plastic bottles, which were sealed and stored at 20 °C for approx. one month. Then the AAS paste was crushed with a jaw crusher. The crushed AAS paste was stored in sealed bottles filled with N_2 to avoid carbonation. After another 2 months, the AAS paste was subsequently ground with a rotating disc mill to a sand-like particle size of maximum 1 mm. As a reference material, OPC paste was prepared with a high-shear mixer and sealed cured at 20 °C in a plastic bag for approximately one month before being crushed and ground to sand like particle size distribution. Until exposure, all sand-like pastes were stored in sealed plastic bags in a desiccator with soda lime and silica gel.

2.2. Equilibrium experiment

An exposure solution with approx. 2 M chloride concentration was prepared by weighing in 58.44 g NaCl to approx. 500 ml of deionized water. This solution was diluted 4 times by mixing 50 vol.% deionized water with 50 vol.% exposure solution resulting in five exposure solutions with different added chloride concentrations ($C_{Cl,added}$).

For the equilibrium experiment, 30 g of the well-hydrated sand-like paste was weighed into 50 ml plastic centrifuge tubes, and 15 ml of the exposure solution was added. For selected exposure concentrations, 2–3 samples were prepared. For each binder, additional reference samples (0.0M) were prepared with 15 ml of deionized water. All samples were stored at 20 °C for approximately one month to reach equilibrium. During this period, the samples were shaken regularly using a mechanical shaker. Then, the liquid phase of the equilibrium samples was extracted by centrifuging at 4000 rpm for 2.5 min. From the OPC samples, approximately 2.5 ml of supernatant could be extracted. In contrast, only 0.2–1.3 ml could be extracted from the AAS0.5 and AAS1.9 samples, although the AAS pastes exhibit a higher free water content (see Section 2.4) and despite the fact, that the 15 ml of exposure solution was used for all equilibrium samples.

Table 1
Properties of CEM I 42.5 and GGBFS (from Ecocem). Chemical composition measured by XRF [w.%].

	CaO	SiO_2	Al_2O_3	Fe_2O_3	MgO	K_2O	Na_2O	TiO_2	P_2O_5	MnO	LOI	Na_2Oeq	SO_3
CEM I	57.90	18.85	5.43	3.33	2.30	1.64	0.06	0.24	0.12	0.08	3.44	1.14	2.00[a]
GGBFS	38.80	36.30	12.80	0.62	7.95	0.60	0.34	0.96	0.02	0.29	1.32	–	0.18

[a] Assumption.

Table 2
Mix design of OPC and AAS paste.

Mix	Binder	Water/binder-ratio	n	M_s
OPC	CEM I	0.47	–	–
AAS0.5	GGBFS	0.47	4%	0.5
AAS1.9	GGBFS	0.47	4%	1.9

Table 3
Evaluation protocol used to determine the chloride binding capacity indirectly using the *equilibrium method* (*EM*).

Evaluation protocol	*EM* Eq. (6)	*EM* Eq. (7)
Analysis	Indirect (liquid)	Indirect (liquid)
Initial chloride concentration	$C_{Cl,init}$	$C_{Cl,added}$
Reference mass	$m_{sample,0}$-$m_{pore,0}$	$m_{sample,0}$
Unit $C_{Cl,b}$	[g Cl/g dry paste]	[g Cl/g moist paste]

The added chloride concentrations ($C_{Cl,added}$) and the equilibrium chloride concentrations of the supernatant ($C_{Cl,eq}$) were determined by potentiometric titration. The titration was conducted with a 916 Ti-Touch titrator from Metrohm using 0.01 M $AgNO_3$ or 0.1 M $AgNO_3$ solutions. Depending on the expected chloride concentration, 0.1–0.2 ml of the supernatant was pipetted into a measurement beaker with 1 ml HNO_3 (65%, diluted 1:10) and 2.5 ml 0.2% polyvinyl alcohol, and then automatically diluted with deionized water before the titration. The chloride concentration of selected supernatants was measured multiple times, for these samples the standard deviation is reported.

Two evaluation protocols for the equilibrium method (EM), summarized in Table 3, were used to determine the chloride binding capacity. The first protocol based on Eq. (6) is commonly used for OPC, while the second protocol based on Eq. (7) resembles the protocol commonly used for AAS pastes. In the latter, the moist mass of the sample ($m_{sample,0}$) is used as the reference mass, rather than the methodologically correct dry mass ($m_{sample,dry}$). This methodologically incorrect evaluation was done to compare the experimental results of *EM* Eq. (7) with the AAS isotherms reported in literature. Isotherms were fitted based on Eqs. (1), (2), and (3).

2.3. Solvent exchange

For the plain sand-like pastes and selected equilibrium samples, after the liquid phase was extracted, the reaction was stopped using solvent exchange. First, any pore solution which could contain free chlorides was removed to prevent the crystallization of ions during solvent exchange [30] ensuring that the remaining solid includes only reaction produces of the paste and no crystalline ions precipitated from the pore solution [36]. To achieve this, the paste was first homogenized with a spatula. Then, 5 ± 0.1 g of the (moist) paste was placed in a 250 ml beaker with approximately 50 ml of deionized water. The suspension was stirred for 3 min and then filtered.

The remaining solids of each sample were then further treated with a double solvent exchange. 100 ml of isopropanol was added to the filtration unit containing the solids. The mixture was stirred for 30 s with a glass rod, left for 5 min, then filtered. This isopropanol treatment was performed twice. Then, 20 ml of diethyl ether was added to the filtration unit, followed by 30 s of stirring and a 5 min rest period before filtration until dry. Diethyl ether is used to minimize the sorption of organics on hydrated paste [36]. The dry sand-like solids were stored overnight by −0.2 bar in a vacuum desiccator. Parts of this were used later for SEM–EDS analysis. On the next day approx 1.7 g of the solids were ground in a porcelain mortar to pass a 63 μm sieve. These ground solids were used for TGA and XRD at the same day to prevent any further reactions.

Table 4
Free and total water content [w.%] of sand-like paste before exposure.

Paste	Free water content	
	$m_{pore,0}$ 40 °C for 10 h	$m_{pore,105C}$ 105 °C for 2 h
OPC	16.15	17.72
AAS0.5	19.78	22.25
AAS1.9	18.66	20.97

2.4. Thermogravimetric analysis

A Mettler Toledo TGA/DSC3+ was used to perform the TGA experiments. To investigate the free water content approx. 250 mg of the sand-like pastes were weighed into 600 μl crucibles and dried while purging 50 ml/min N_2 using two settings: Drying at 40 °C for 10 h, which might accelerates some reactions within the innerpart of the particles due to the slow drying process. Drying at 105 °C for 2 h, which is a common approximation of the free water content, even though hydration phases such as ettringite and C–(N)–(A)–S–H are also known to lose water at these conditions. The free water content of the well-hydrated binders is presented in Table 4. As expected, the free water content measured by 105 °C was about 2 w.% higher than that measured by 40 °C.

All paste samples were characterized by TGA from 40 °C to 950 °C with a rate of 10 °C/min, while being purged with with 50 ml/min N_2. The TGA results are presented as mass loss (TG) and the derivative of the mass loss per K (DTG) as functions of temperature, where the mass losses are normalized to the initial sample mass.

The AFm phases monosulfate and monocarbonate release interlayer water from their octahedral layers in the temperature ranges of approximately 250–350 °C and 200–300 °C, respectively [36]. The formation of Friedel's salt requires the presence of such AFm phases prior to chloride exposure. The thermal decomposition of synthesized Friedel's salt ($Ca_4Al_2(OH)_{12}Cl_2 \cdot 4H_2O$) shows two main DTG peaks at 30–180 °C and 230–410 °C, with the second peak typically used to identify Friedel's salt. For OPC systems the quantity of Friedel's salt can be determined from the content of the main layer water (230–410 °C) [16,45]. For AAS systems the mass loss of NaCl-exposed samples in the range 230–410 °C is attributed to hydrotalcite and, if formed, Friedel's salt. For this, the mass loss of the NaCl-exposed sample is corrected by the mass loss of the water exposed (*0.0 M*) sample [45,46]. The quantification of Friedel's salt using Eq. (9) is therefore just a rough estimate.

$$m_F = \frac{M_{Friedel}}{6 \cdot M_{H_2O}} \cdot \left(\frac{m_{NaCl,230°C} - m_{NaCl,410°C}}{m_{NaCl,105°C}} - \frac{m_{0.0M,230°C} - m_{0.0M,410°C}}{m_{0.0M,105°C}} \right) \quad (9)$$

where m_F [g/g dry sample] is the mass fraction of Friedel's salt content of the sample, $m_{230°C} - m_{410°C}$ is the mass loss in the range of 230–410 °C, $M_{Friedel}$ = 561.3303 g/mol and M_{H_2O} = 18.02 g/mol are the molar masses of Friedel's salt and water.

For AAS systems, the mass loss in the range of 230–410 °C can also be associated with hydrotalcite, which also loses six water molecules representing the main layer water [16,47], which overlaps with the water release of AFm phases. The quantification of hydrotalcite using Eq. (10) is in the presence of AFm phases therefore an overestimation.

$$m_{Ht} = \frac{M_{Ht}}{6 \cdot M_{H_2O}} \cdot \frac{(m_{0.0M,230°C} - m_{0.0M,410°C})}{m_{0.0M,105°C}} \quad (10)$$

where m_{Ht} [g/g dry sample] is the mass fraction of hydrotalcite of the sample and $M_{Ht} = 443.18$ g/mol [16].

The upper bound of chemical bound water of the paste after solvent exchange $m_{H,chem}$ [w.% dry sample] is calculated based on the weight loss between 105 °C and 950 °C:

$$m_{H,chem} = \frac{m_{105°C} - m_{950°C}}{m_{40°C}} \cdot 100\% \quad (11)$$

2.5. X-ray diffraction

X-ray diffraction (XRD) was used to identify crystalline phases and phase changes due to chloride binding. A Bruker D8 A25 DaVinci X-ray Diffractometer equipped with a LynxEye SuperSpeed Detector detector, with CuKα radiation (wavelength of 1.54 Å) was used. The scans ranged from 5–55° 2θ using a step size of 0.01° 2θ and had the total measuring time of 87 min per sample.

Approximately 0.5 g of each ground paste was back loaded into sample holders and measured immediately. The sand-like paste before exposure was ground to pass a 63 μm sieve at the same day of XRD measurement. The paste after the equilibrium experiments was treated in the same way as the TGA samples (washing and solvent exchange).

Additionally, moist paste after the equilibrium experiments was measured to investigate the effect of water loss due to the solvent exchange. After taking solid for the solvent exchange from the sample tubes, approx. 3 g of moist sand-like paste was taken for an additional XRD measurement. The moist sand-like sample was quickly ground in a porcelain mortar to achieve a homogeneous fine paste. Then the moist paste was front loaded into sample holders and covered with Kapton foil to prevent the drying of the sample while measurement.

External standard method is used to quantify different phases (crystalline and amorphous) in the specimens using Rietveld analysis further described in Appendix A.5.

2.6. SEM-EDS

Scanning Electron Microscopy with Energy-Dispersive X-ray Spectroscopy (SEM–EDS) is used to investigate the paste before and after exposure. First, Backscattered Electron Images (BSE) images and Energy-Dispersive X-ray Spectroscopy (EDS) point analysis was performed on the solvent-exchanged paste grains, dusted directly onto adhesive double-sided carbon tape using FIB–SEM, Zeiss CrossBeam 350 KMAT focused ion beam scanning electron microscope with accelerating voltage of 15 kV and spectrum area counts above 1×10^6 for all measurements, ensuring reliable quantification. Energy Dispersive X-ray Spectrometry (EDS) analysis was performed by a UltimMax100 silicon drift detector from Oxford Instruments. The EDS data processing is done using AZtec 6.2 SP2 software, including normalization, correction for window artifacts as well as sum peaks and pulse pile up correction.

Next, approximately 0.5 g of solvent-exchanged paste grains were placed in a 2 mL tapered plastic vial and impregnated with 1 mL of Epo-Tek 301 epoxy (Epoxy Technology Inc.). The epoxy is chloride-containing, but it does not affect the point EDS point analysis as no chloride is observed in the samples which were not in contact with NaCl solution (see Appendix A.6). The vials were evacuated at 0.1 bar to remove entrapped air and subsequently cured under 2.5 bar overpressure. After hardening, the vials were cut longitudinally with an ethanol-cooled diamond saw, the plastic removed, and three epoxy–sample halves were re-embedded in a 30 mm round mold with the cut surfaces facing downward. Following vacuum impregnation and pressure curing, the resulting epoxy puck was lathed flat on the top surface. The bottom surface was ground using 120 and 220 grit diamond pads and polished sequentially with 6, 3, 1, and 0.25 μm alcohol-based diamond suspensions using a Struers Tegramin-30 grinding and polishing machine, with ethanol as lubricant. For EDS maps and point analysis of the polished samples a Hitachi S-3400 N scanning electron microscope equipped with an EDS-detector from Oxford Instruments was used. EDS was performed with a emission current of approx. 75–100 μA and accelerating voltage of 15 kV. BSE images, EDS maps and point analysis were acquired with a working distance of approx. 10 mm. The elemental maps for Al, Na, Ca, Mg, C, Si, Fe, K and Cl were used to select regions for point scan analyses. Maps were acquired at 75× and 750× magnification, while point analysis is conducted only at 750× magnification. For the point analysis (ratio plots), points used to determine the atomic ratio were taken from the middle of the particle, not from the (leached) rim near the surface.

2.7. Thermodynamic simulation

In the thermodynamic modelling, congruent OPC and slag dissolution was assumed, and proportional additions of SiO_2, CaO, Al_2O_3, MgO, Fe_2O_3, Na_2O, K_2O, and SO_3 were used. O_2 was included in the system, while no addition of C was considered, assuming that carbonation did not occur. The simulations were performed using the Cemdata18 database [48] combined with the Zeolite21 database [49,50] and the CASH+ model [51], which was extended to account for the uptake of alkali metals [52] and alumina [53]. The CASH+ model was chosen, because it correlates better with the SEM–EDS C–(N)–(A)–S–H composition of the AAS paste as compared to the CNASH solid solution model available in cemdata18. The zeolite A4 from Zeolite21 database was used as a proxy for the N–A–S–H phase. The temperature and pressure were set to 20 °C and 1 bar, respectively. For alkali-activated slag systems, the high ionic strength at early ages often suggests the use of the Pitzer ion activity model. However, comparisons between calculations based on the Pitzer model [54] and the extended Debye–Hückel model [55] have shown that the choice of ion activity model has only a minor influence on the predicted phase assemblage in alkali-activated slag systems [42]. Therefore, the extended Debye–Hückel (Helgeson) model is used in this study for both, AAS and OPC paste. To simulate chloride binding, the a_i and b_γ parameters were set at 3.72 A and 0.64 kg/mol, respectively, and NaCl was used as the background electrolyte for hydration systems. Gibbsite and quartz from cemdata18 were suppressed as their occurrence in the system investigated is unfavourable to occur. In addition, ettringite and monosulphate solid solutions were suppressed to favour occurrence of pure phases. To calculate the volume of unreacted phases, the density of OPC and slag were estimated to be 3.15 and 2.8 g/cm^3, respectively

In the equilibrium simulation, the degree of hydration (DoH) of the OPC was set to 70%, based on the Parrot and Killoh model [56]. For this the fineness of OPC was assumed to be 390 m^3/kg. In the case of alkali-activated slag (AAS), Caron et al. [42], using slag from the same supplier but a different activator, reported slag dissolution between 48% and 55% after 56 days, depending on the silicate modulus (M_s) of the activator solution. Higher M_s values lead to a lower pH [57], which can reduce the degree of reaction [42]. In addition, a higher silicon concentration in the activator may limit further slag dissolution [42]. In the present study, the activator solution for AAS1.9 contains a relatively high silicon content, which likely contributes to a lower degree of hydration. Comparable findings were reported by Haha et al. [58] (48% after 180 days), Le Saoût et al. [59] (52% after 28 days and 54% after 100 days), and Bernal et al. [60] (45%, 58%, and 79% after 56 days for three different slags). Based on these observations, the DoH for the GGBFS in both AAS pastes was estimated to be approximately 60%.

Table 5
Prediction protocol used to determine the bound chloride content from thermodynamic simulation.

Prediction protocol	GEMS Eq. (12)	GEMS Eq. (6)	GEMS Eq. (7)
Similar to	Microstructural quantification	*EM* Eq. (6)	*EM* Eq. (7)
Analysis	direct (solid)	indirect (liquid)	indirect (liquid)
Evaluating	$m_{Friedel}$ and m_{Kuzel}	$C_{Cl,eq}$	$C_{Cl,eq}$
Reference mass	$m_{sample,0}$-$m_{pore,0}$	$m_{sample,0}$-$m_{pore,0}$	$m_{sample,0}$
Unit $C_{Cl,b}$	[g Cl/g dry paste]	[g Cl/g dry paste]	[g Cl/g moist paste]

Chloride binding is simulated based on the laboratory conditions in the *equilibrium method*. The solid/liquid ratio ($m_{sample,0}/V_{add}$ = 30 g moist paste/15 ml NaCl sol.) is chosen to be same as in equilibrium experiment described above. To determine chloride binding isotherms, the concentration of the added solution ($C_{Cl,add}$) was stepwise increased, while the DoH was assumed to be constant. First, the total mass of the paste consisting of the solid phase and the pore solution ($m_{sample,0} = m_{sample,dry} + m_{pore,0}$) was determined. Then, the composition of the added solution was adjusted, while the volume of the added NaCl solution ($V_{add} = V_{H2O,added} + V_{Cl,added} + V_{Na,added}$) was kept constant to match the solid-to-liquid ratio. Based on the thermodynamic equilibrium, the resulting $C_{Cl,eq}$, $m_{Friedel}$ and m_{Kuzel} were predicted.

In Table 5, the 3 prediction protocols used in this study to evaluate the thermodynamic simulation are summarized. The first is *GEMS* Eq. (12), which involves the direct determination of the mass of chemically bound chlorides ($C_{Cl,chemical}$). Here, $C_{Cl,chemical}$ [g Cl/g dry paste] is directly determined from the masses of the chloride-containing phases:

$$C_{Cl,chemical} = C_{Cl,Friedel} + C_{Cl,Kuzel} = \frac{m_{Friedel} \cdot \frac{2 \cdot M_{Cl}}{M_{Friedel}}}{m_{sample,0} - m_{pore,0}} + \frac{m_{Kuzel} \cdot \frac{M_{Cl}}{M_{Kuzel}}}{m_{sample,0} - m_{pore,0}} \quad (12)$$

where $m_{Friedel}$ and m_{Kuzel} [g] are the masses of Friedel's salt and Kuzel's salt predicted by the thermodynamic model and, $M_{Friedel}$=561.33 g/mol and M_{Kuzel}=1042.22 g/mol [48] are the correspondence molar masses.

The other prediction protocols are similar to the *equilibrium method*, where the chloride binding capacity is determined indirectly based on the predicted chloride concentration of the equilibrium solution ($C_{Cl,eq}$). For this, Eqs. (6) and (7) are used to indirectly determine $C_{Cl,b}$.

2.8. Summary of the experimental program

An overview of the experimental program is given in Fig. 4. The paste sample before exposure is called *plain*, it was not exposed to water nor to NaCl-solution. For all exposed sample, the name is chosen based on the measured equilibrium chloride concentration ($C_{Cl,eq}$). For instance, the AAS0.5 sample with $C_{Cl,eq}$ = 0.39 mol Cl/l is called *AAS0.5 0.39M*, while the AAS0.5 sample exposed to water is called *AAS0.5 0.0M*. By default solids where dried with solvent exchange. Only samples labelled *wet* are measured in a moist state, directly taken after exposure.

3. Results

3.1. Chloride binding isotherms

The measured chloride concentrations and the sample names of all solid samples are given in Tables 6 and 7, respectively. For the added chloride concentration of 1.81 mol/l, each equilibrium concentration was measured three times, demonstrating a good repeatability of the equilibrium concentration measurements.

It has to be noted, the sand-like grains of the AAS paste agglomerated over time but were regularly dispersed again by tapping and automated vibration, allowing them to remain freely suspended in the solution. The agglomeration was more pronounced for the AAS paste compared to the OPC paste.

In Fig. 5, the chloride binding isotherms based on the evaluation protocols given in Table 3 are compared. For AAS, accounting for the initial water content as done in *EM* Eq. (6) leads to a negative chloride binding, which is not possible from mass conservation perspective. This will be further discussed using results of thermodynamic modelling. Neglecting the initial water content of the sample as done in *EM* Eq. (7), the AAS pastes exhibit a linear binding behaviour. Compared to the OPC paste, the AAS pastes have a lower chloride binding capacity. This is contradictory to the findings of the literature review discussed in Fig. 3.

In Fig. 6, the OPC binding isotherm obtained in this study is compared with those reported for similar pastes in the literature. The OPC isotherm using $C_{Cl,b}$ based on *EM* Eq. (6) shows good agreement with studies that increased the degree of hydration by producing "moist sand" [29–31], as illustrated in Fig. 6(a). If the initial water content is neglected and Eq. (7) is applied, the resulting isotherm corresponds closely to those from studies using the same simplification [26,28], as illustrated in Fig. 6(b). A comparison between Figs. 6(a) and 6(b) indicates that the water-to-binder ratio (w/b) has a stronger influence on the binding capacity when the initial water content is taken into account.

The AAS pastes examined in this study exhibit a lower binding capacity than those reported in the literature, when the initial water content is neglected as shown in Fig. 7. This difference might be due to different activator compositions and due to the fact, that the reference mass in *EM* Eq. (7) was the mass of the moist sample where no drying procedure as applied, which decreases the calculated binding capacity.

3.2. XRD

Fig. 8 shows XRD patterns for all samples. Both AAS pastes are largely amorphous, containing a broad C–(N)–(A)–S–H peak and the unreacted slag. For all AAS pastes, the amount of crystalline phases is close to detection limit for quantification using Rietveld refinement (see Appendix A.5). Furthermore, the peak position of layered hydroxide phases (hydrotalcite (Ht), monosulfoaluminate (Ms), Friedel's salt(Fs)) shifts depending on the binder composition and their chloride content [13,18,61], which increases the uncertainty in Rietveld quantification.

Hydrotalcite ($Mg_6Al_3(OH)_{18}(CO_3)_{1.5} \cdot 4.5\,H_2O$) is detected with distinct peaks only in the AAS0.5 samples, with Rietveld refinement indicating contents of about 1.3 w.%. In contrast, no hydrotalcite was detected by Rietveld refinement in the AAS1.9 samples. Monosulfoaluminate ($Ca_4Al_2SO_{10} \cdot 16\,H_2O$) [62] is absent in the *plain* samples, but present in all samples stored in water (*0.0M*) or NaCl solution, where the peaks are more intense in the *wet* samples compared to the solvent-exchanged ones. This finding is consistent with earlier observations, which showed that monosulfoaluminate phases undergo structural changes during storage in NaCl solution and subsequent drying, favouring the more hydrated variant [63], which suggests that water may be permanently bound within this phase. However, from a thermodynamic view monosulfoaluminate phases are not expected to exist in NaCl-exposed samples, as the Friedels's salt formation is favoured (see Section 2.7). However, Friedel's salt is detected exclusively in samples exposed to NaCl solution and is better visible in *wet* samples. In AAS1.9, a Friedel's peak at 11.3° in the *AAS1.9 1.38M wet* sample is detected, whereas no distinct peak was observed at *AAS1.9 0.42M wet* sample. Rietveld quantification on the solvent-exchanged samples yields a Friedel's salt of 0.11 w.% for the *AAS1.9 0.42M*

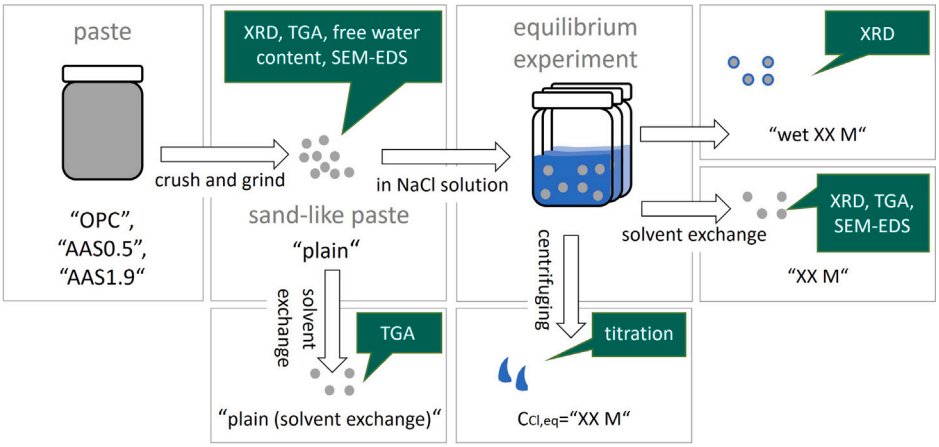

Fig. 4. Overview of experimental program and sample naming.

Table 6
Measured equilibrium chloride concentration $C_{Cl,eq}$ [mol/l] of the corresponding exposure solutions $C_{Cl,added}$ [mol/l]. Standard deviation is given in brackets, if equilibrium chloride concentration was measured multiple times.

$C_{Cl,added}$ [mol/l]	$C_{Cl,eq}$ [mol/l]		
Exposure solution	OPC	AAS0.5	AAS1.9
0.14	–	0.1155	0.1187
0.25	0.0893	0.2021	0.2418
0.54	0.2692; 0.2679; 0.2670	0.3972; 0.3965	0.4289
1.08	–	–	0.7805
1.81	1.2040 (0.0143)	1.2598; 1.2695 (0.0252)	1.3854 (0.0013)

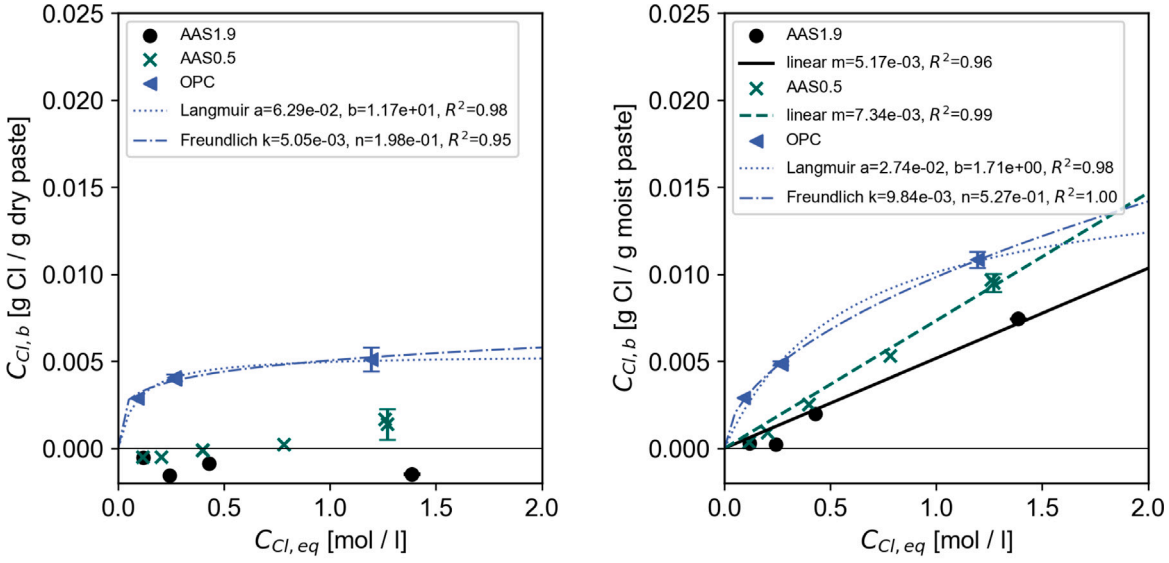

(a) $C_{Cl,b}$ with *EM Eq.* (6) (b) $C_{Cl,b}$ with *EM Eq.* (7)

Fig. 5. Chloride binding isotherms measured by the *equilibrium method* and evaluated based on the evaluation protocols given in Table 3: (a) $C_{Cl,b}$ with *EM* Eq. (6) (b) $C_{Cl,b}$ with *EM* Eq. (7).

sample and 0.74 w.% for the *AAS1.9 1.38M* sample. For AAS0.5 the *wet* samples exposed to NaCl solution showed peaks at 11.3°, 22.5° and 31.1°, which can be associated with Friedel's salt formation. Rietveld refinement of solvent exchanged samples giving values between 0.74 and 0.97 w.% for AAS0.5.

The OPC samples contain a larger variety of crystalline phases. The unhydrated clinker phases (Belite, Alite, Ferrite, Periclase) account for roughly 25 w.% of the total content, corresponding to a DoH of about 75%, confirming the estimated DoH. Portlandite, ettringite, hemicarbonate, monocarbonate, quartz, Belite, Alite, Ferrite, and Periclase were identified in all mixes. Friedel's salt is also detected in the *OPC 0.26M* samples, with Rietveld refinement giving approximately 1.91 w.%. This is significantly more as detected in the AAS pastes (*AAS1.9 0.42M* and *AAS0.5 0.39M*), which were also exposed to 0.54 M NaCl solution (see Table 7), indicating a higher chemical chloride binding capacity of OPC paste.

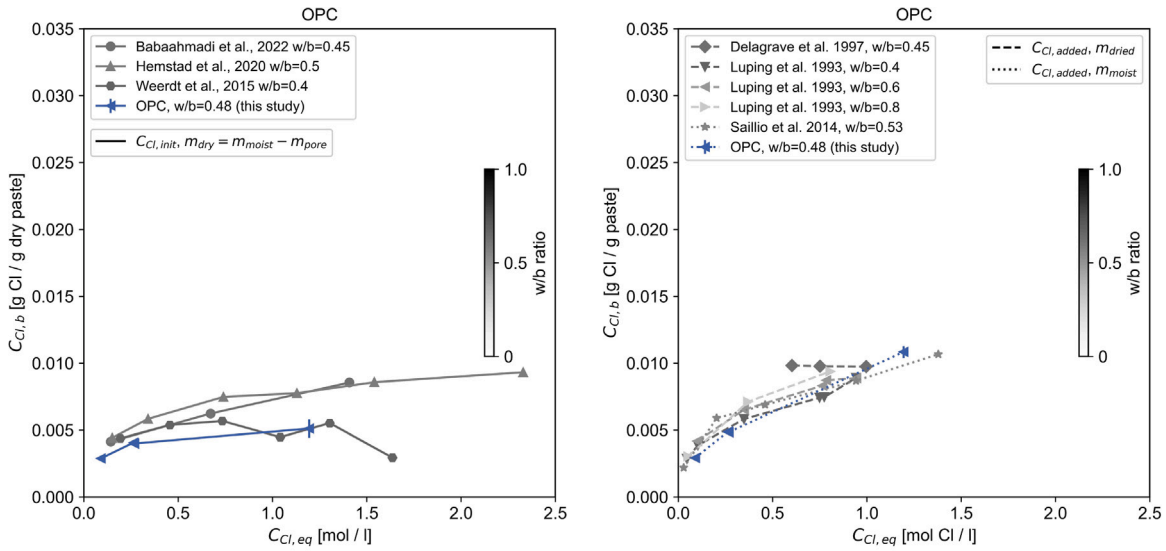

(a) $C_{Cl,b}$ with *EM Eq.* (6) (b) $C_{Cl,b}$ with *EM Eq.* (7)

Fig. 6. Comparison of OPC chloride binding isotherm based on different evaluation protocols: (a) *EM* Eq. (6) with chloride binding isotherm from OPC studies [29–31] (b) *EM* Eq. (7) with chloride binding isotherm from OPC studies [21,26,28].

Table 7
Sample name of paste taken from the corresponding exposure solutions $C_{Cl,added}$ [mol/l]. The sample name includes the measured equilibrium concentration $C_{Cl,eq}$.

Exposure solution	OPC	AAS0.5	AAS1.9
0.00	*OPC 0.0M*	*AAS0.5 0.0M*	*AAS1.9 0.0M*
0.54	*OPC 0.26M*	*AAS0.5 0.39M*	*AAS1.9 0.42M*
1.81	–	*AAS0.5 1.26M*	*AAS1.9 1.38M*

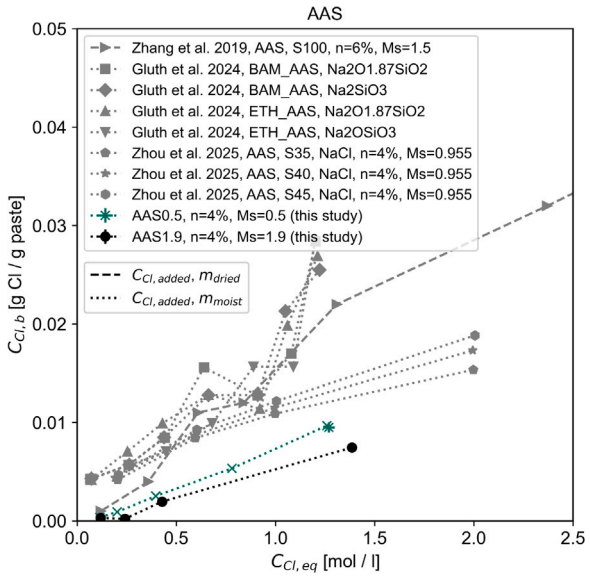

Fig. 7. Comparison of isotherm of this study with AAS isotherms based on the evaluation protocol *EM* Eq. (7) with chloride binding isotherm from AAS studies [15,19,35].

3.3. TGA

In Fig. 9(a), the DTG curves of *plain* samples, the *plain* samples after solvent exchange and water-exposed *0.0 M* samples (after solvent exchange) are compared. For OPC, the main peak is primarily attributed to the decomposition of C–S–H and with a lesser contribution due to the decomposition of ettringite and AFm phases (monocarboaluminate, monosulfoaluminate). Whereas for the AAS pastes, the main peak is primarily attributed to the decomposition of C–(N)–(A)–S–H. Comparing the *plain* samples to the solvent exchanged samples, all mixes show notable differences in their main peaks, which are caused by the solvent exchange process of the samples. However, comparing the solvent exchanged samples, the *OPC 0.0 M* sample might indicate limited leaching of the C–S–H, while the portlandite content remains stable after water exposure. In contrast, both *AAS 0.0 M* samples indicate a slight increase in the C–(N)–(A)–S–H peak compared to the *AAS plain* solvent exchanged sample.

The DTG curves of the chloride-exposed samples (after solvent exchange) are shown in Figs. 9(b) to 9(d). For the OPC sample in Fig. 9(b), a change in the mass loss curve is observed between 230–410 °C, corresponding to the release of the six main layer water molecules during Friedel's salt decomposition [36,45].

For the AAS pastes, the Friedel's peak is overlapping with the hydrotalcite peaks and, if existing, monosulfoaluminate peak. As several phases are decomposing in this range, a quantification of Friedel's salt based on Eq. (9) is therefore not reliable. For AAS0.5, illustrated in Fig. 9(c), the peak in the range 230–410 °C shifts with increasing chloride concentration to lower temperatures, which is accompanied by a shift of the mass loss in the range of 150–250 °C. This indicates changes in the layered hydroxide phases (hydrotalcite, monosulfoaluminate, Friedel's salt). As illustrated in Fig. 9(d), the layered hydroxide phases of the AAS1.9 paste seem less affected by chloride exposure. Only for the *1.38M* sample, the mass loss in the 230–410 °C range is altered. The quantification of hydrotalcite and Friedel's salt based on TGA analysis are summarized in Appendix A.4.

The chemically bound water content of the paste $m_{H,chem}$ is illustrated in Fig. 10. For the OPC samples, the amount of chemically bound water decreases slightly after the equilibrium experiments. In contrast, both AAS pastes show an increase in chemically bound water content with increasing NaCl concentration in the exposure solution. This suggests that additional water-binding reactions occurred during exposure. The effect is more pronounced for the AAS0.5 paste than for the AAS1.9 paste.

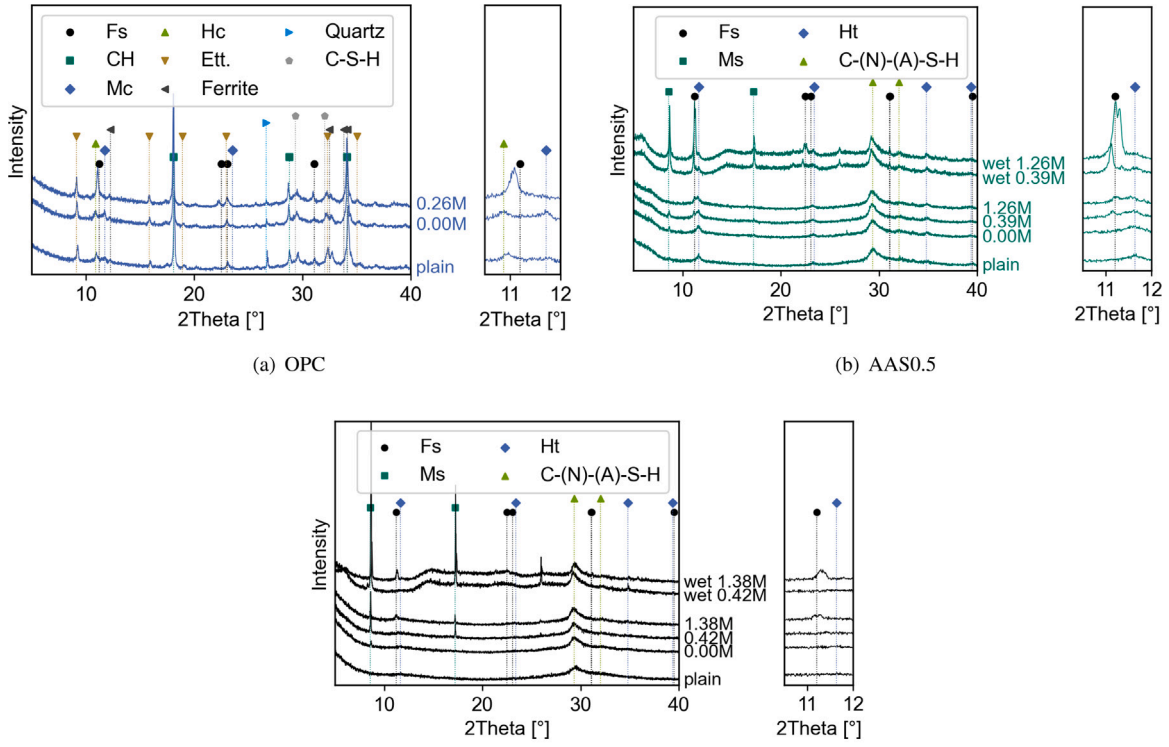

(a) OPC

(b) AAS0.5

(c) AAS1.9

Fig. 8. XRD patterns of OPC and AAS paste before exposure to NaCl solution (*plain*) and at different equilibrium concentrations $C_{Cl,eq}$ measured after solvent exchange or at *moist* samples, before solvent exchange (*wet*). Labelling of peaks based on Appendix A.5.

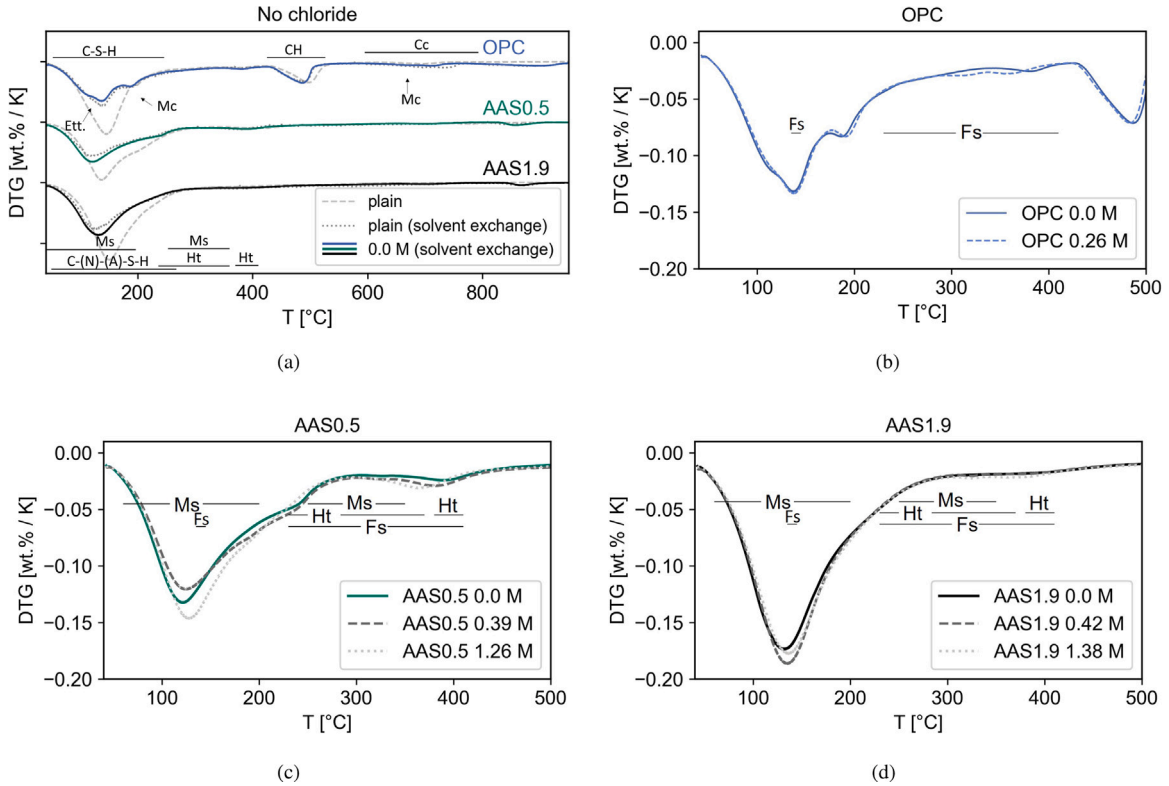

(a)

(b)

(c)

(d)

Fig. 9. TGA of OPC and AAS paste before exposure to NaCl solution (plain) and at different equilibrium concentrations $C_{Cl,eq}$. Ht = hydrotalcite, Ett. = ettringite, CH = portlandite, Cc = calcite, Mc = monocarbonate, Ms = monosulfoaluminate, Fs = Friedel's salt. Phase annotations based on Scrivener et al. [36].

Table 8
Elemental molar ratios obtained from SEM–EDS measurements compared with reference chloride-containing AFm phases (Cl–AFm).

Sample	Phase	Ca/Al	Cl/Al	S/Al	Si/Al
OPC 0.26M (polished)	Cl–AFm	1.93	0.58	0.03	0.09
AAS0.5 1.26M (grain)	Cl–AFm	1.68	0.37	0.00	0.18
AAS1.9 1.38M (grain)	Cl–AFm	1.82	0.23	0.38	0.39
Ideal Friedel's salt [48]	$Ca_4Al_2(OH)_{12}Cl_2 \cdot 4H_2O$	2.00	1.00	0.00	0.00
Ideal Kuzel's salt [48]	$Ca_4Al_2Cl(SO_4)_{0.5}(OH)_{12} \cdot 6H_2O$	0.50	2.00	0.25	0.00

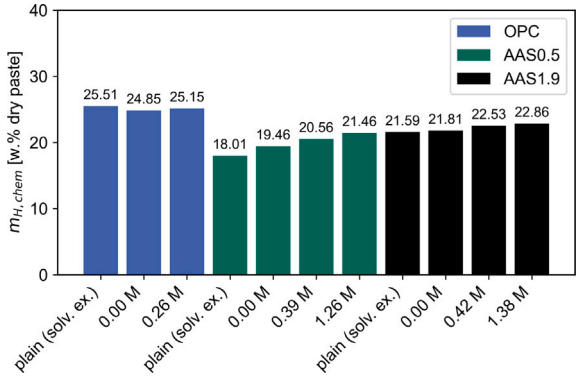

Fig. 10. Chemical bound water $m_{H,chem}$ of samples (after solvent exchange) according to Eq. (11).

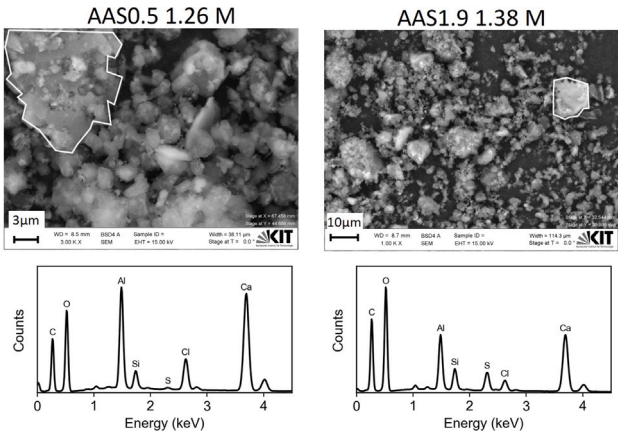

Fig. 11. SEM–EDS analysis on grains of AAS paste: Cl-containing AFm phase.

3.4. SEM-EDS

SEM–EDS analysis of individual grains revealed the presence of chloride-containing AFm phases in the chloride-exposed AAS samples. As illustrated in Fig. 11, these phases exhibit high Al, Ca, and Cl contents and low Si content. The elemental ratios given in Table 8 indicate that the composition in AAS0.5 resembles Friedel's salt, whereas AAS1.9 contains sulphate and shows a lower Cl/Al ratio, resembling Kuzel's salt. This suggests a lower chloride-binding capacity of chloride-containing AFm phases in the AAS1.9 paste.

Elemental mapping of polished samples are illustrated in Fig. 12. The Cl maps show a constant intensity of the chloride-containing resin, while also Cl is also detected in the centre of large particles, indicating that equilibrium was reached. In contrast, the maps of the *plain* paste grains before exposure and after exposure to water (illustrated in Appendix A.6) only show Cl in the resin.

In all NaCl-exposed samples, paste particles exhibit rims enriched in Na and depleted in Cl. Similar rims are observed after water exposure (see Appendix A.6), whereas they are absent in *plain* samples (see Appendix A.6), suggesting that rim formation is driven by exposure-induced leaching, likely involving Ca.

Based on EDS point analysis (details given in Appendix A.6), AAS pastes mainly consist of C–(N)–(A)–S–H, hydrotalcite, and unreacted slag. For the AAS paste, the exposure to water alters the composition of the C–(N)–(A)–S–H phase even in the middle of the particle as illustrated in Fig. 13. Na is leached from the C–(N)–(A)–S–H phase, more strongly in water than in NaCl solution. NaCl exposure appears to induce segregation into Ca-rich and Si-rich domains. This indicates that the (physical) chloride binding occurs in a chemically altered C–(N)–(A)–S–H phase, rather than the initial reaction product.

The hydrotalcite-like phase shows no measurable change in Mg/Al ratio upon exposure to water or NaCl solution as illustrated in Fig. 14. Both, AAS0.5 and AAS1.9, exhibit a Mg/Al ratio of about 1.8, which is governed by the slag composition, the main source of both Mg and Al. Comparable Mg/Al ratios for hydrotalcite-like phases have been reported previously [13,64].

SEM–EDS point analyses to identify the dominant chloride-binding phases is illustrated in Fig. 15. As illustrated in Fig. 15(a), chloride in the *OPC 0.26M* sample is primarily associated with chloride-containing AFm phase (Cl/Al ≈ 0.58) and, to a lesser extent, with C–S–H (Cl/Ca ≈ 0.05). The detected chloride content in the chloride-containing AFm phase is therefore only half of the theoretical Friedel's salt composition (see Table 8). This has been observed before [30,65].

In contrast to the *OPC 0.26M* sample, high chloride concentrations in the polished AAS samples are accompanied by an increase in Mg indicating chloride binding to hydrotalcite, as illustrated in Fig. 15(b). Furthermore, the C–(N)–(A)–S–H phases contributes to chloride binding in the AAS samples as illustrated in Fig. 15(c). This is in agreement with other studies reporting physical chloride binding in C–(N)–(A)–S–H phase [15–17,66,67] and hydrotalcite [16–20]. No clear trend towards chloride-containing AFm in AAS pastes is observed in the polished AAS samples, as they are maybe finely intermixed with the C–(N)–(A)–S–H phase or are missed in the random point analysis. Though, the presence of such phases cannot be excluded as they where detected on the unpolished grains (Fig. 11).

As illustrated in Figs. 15(b) and 15(c), the Cl/Ca and Cl/Al ratio of the *AAS1.9 1.38M* sample is higher as of the *AAS0.5 1.26M* sample. This is contradictory to the measured isotherms (see Fig. 5), where the binding capacity of AAS0.5 was found to be higher. Furthermore, the hydrotalcite of the *AAS1.9 1.38M* sample has a higher chloride content compared to its C–(N)–(A)–S–H phase. The discrepancy between the SEM–EDS results and the binding isotherms remains unexplained.

3.5. Thermodynamic modelling prediction

Predictions of phase assemblage for AAS and OPC paste from thermodynamic modelling for different NaCl concentration exposure are shown Fig. 16. The predicted equilibrium chloride concentration $C_{Cl,eq}$ does not align with experimental values at the same added solution concentration, because the thermodynamic model does not account for the chloride uptake in hydrotalcite, C–(N)–(A)–S–H or zeolite precursors such as Sodalite. It only accounts for bound chlorides in AFm

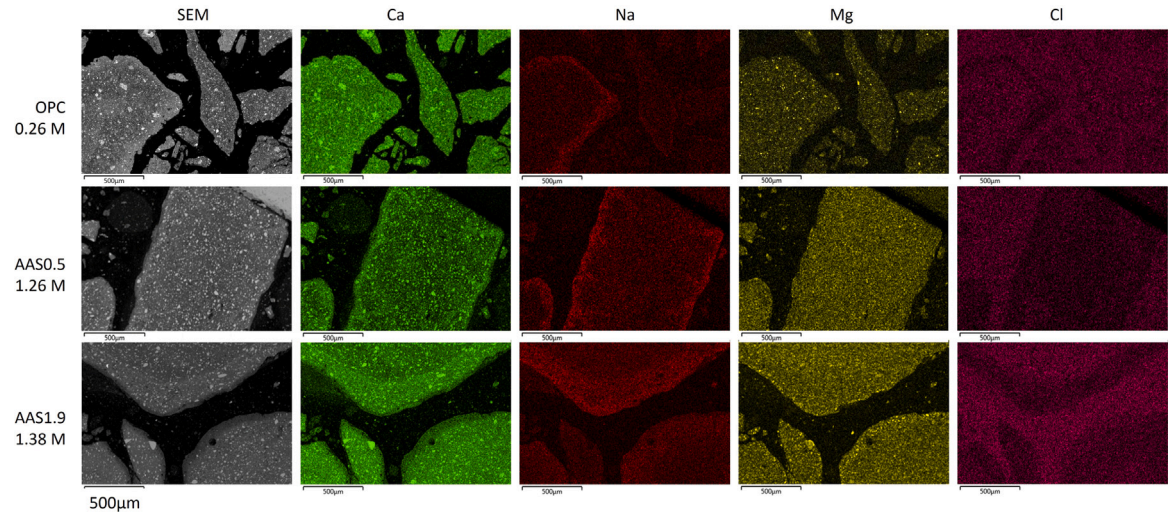

Fig. 12. SEM–EDS maps of polished samples measured with 75× magnification of OPC, AAS0.5 and AAS1.9 samples exposed to NaCl solution. Colour gradient for relative comparison within one image. Note that epoxy resin between grains includes Cl.

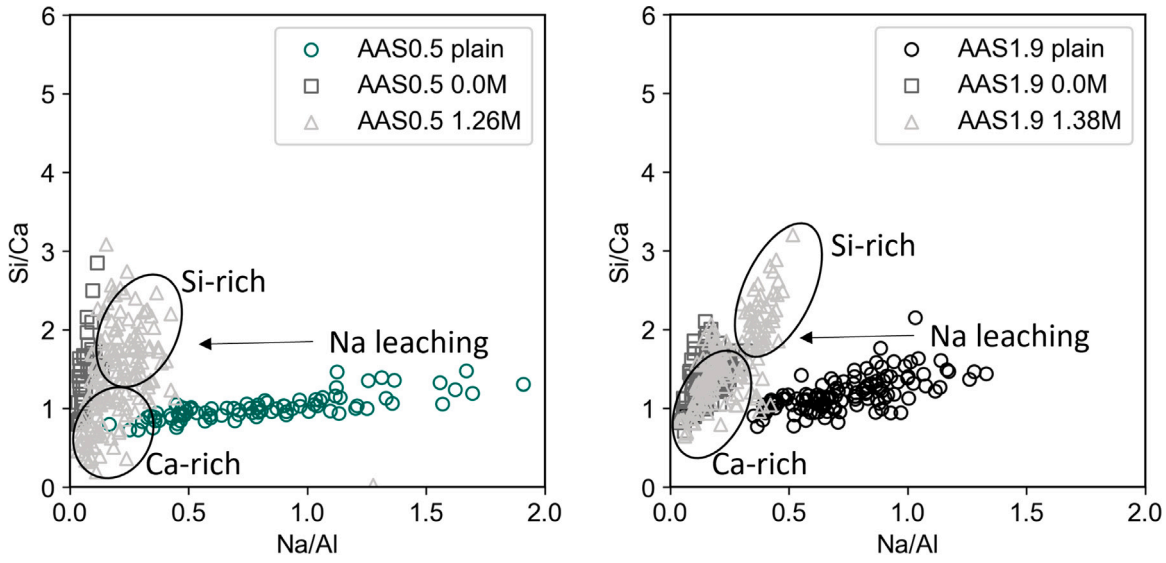

(a) AAS0.5 (b) AAS1.9

Fig. 13. Na/Al vs. Si/Ca ratio of SEM–EDS point analyses of polished samples with 750× magnification. Samples before exposure (*plain*), after water (*0.0M*) exposure or NaCl solution ($C_{Cl,eq}$ = *1.26M* or *1.38M*).

phases. All subsequent comparisons are therefore made at equilibrium conditions based on the same $C_{Cl,eq}$.

For the OPC paste illustrated in Fig. 16(a), the formation of Kuzel's salt and its subsequent transformation into Friedel's salt is predicted, which is in good agreement with other studies [11,29]. For the AAS0.5 paste illustrated in Fig. 16(b), minor phase changes such as the increasingly formation of Friedel's salt with increasing $C_{Cl,eq}$ are predicted. For the AAS1.9 paste, no formation chloride-containing AFm phases is predicted, as illustrated in Fig. 16(c). In contrast to OPC, some of these phase transformations in AAS are reversible, such as the formation of straetlingite or N–A–S–H. For the AAS pastes, the mass of pore solution decreases slightly with increasing NaCl content. Consequently, the predicted liquid volume decreases by approximately 2–2.5 vol% with increasing equilibrium concentration up to 2 mol/l (see Appendix A.7). For the given degree of hydration (DoH = 0.6), this effect is more pronounced in AAS0.5 paste than in AAS1.9 paste. In contrast, the predicted volume reduction in OPC paste is approximately twice that observed for the AAS pastes, while the mass of pore solution is predicted to slightly increase.

4. Discussion

4.1. Comparison of bound chloride content

The bound chloride content determined with different direct and indirect methods is illustrated in Fig. 17. A detailed description of the parameters used for quantification is given in Appendix A.8.

For the *OPC 0.26*M sample, TGA quantification predicts by far the lowest binding capacity. The thermodynamic simulation evaluated based on *GEMS* Eq. (12) predicts a similar amount of chloride bound in Friedel's salt as the *XRD+EDS* quantification, although the latter assumes only half of the theoretical chloride binding capacity of Friedel's salt. Based on *XRD+EDS* quantification, the chloride binding in chloride-containing AFm phase dominates over physical chloride binding of the C–S–H phase.

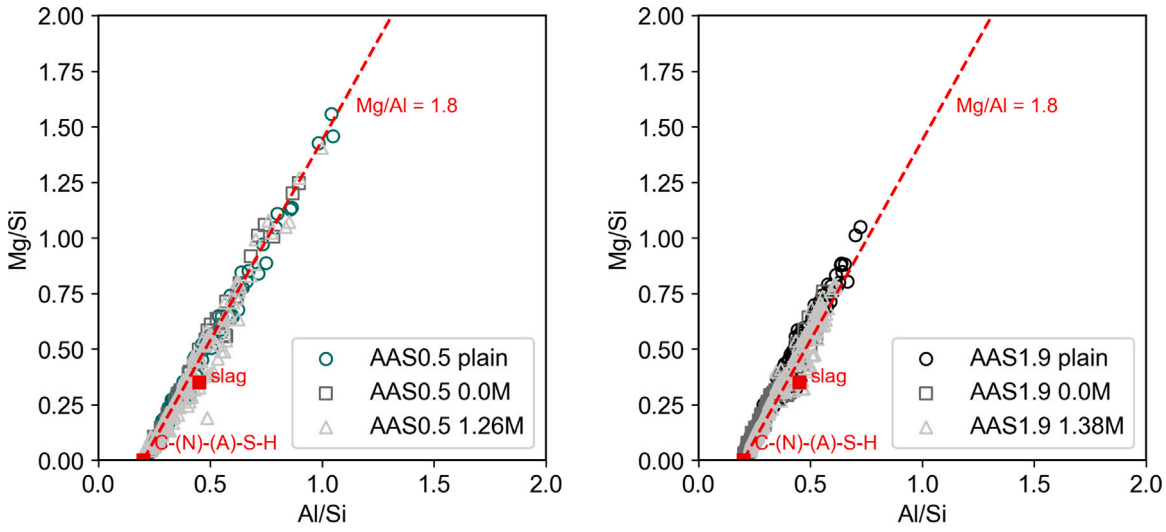

(a) AAS0.5 (b) AAS1.9

Fig. 14. Al/Si vs. Mg/Si ratio of SEM–EDS point analyses of polished samples with 750× magnification. Samples before exposure (*plain*), after water (*0.0M*) exposure or NaCl solution exposure ($C_{Cl,eq}$ = *1.26M* or *1.38M*).

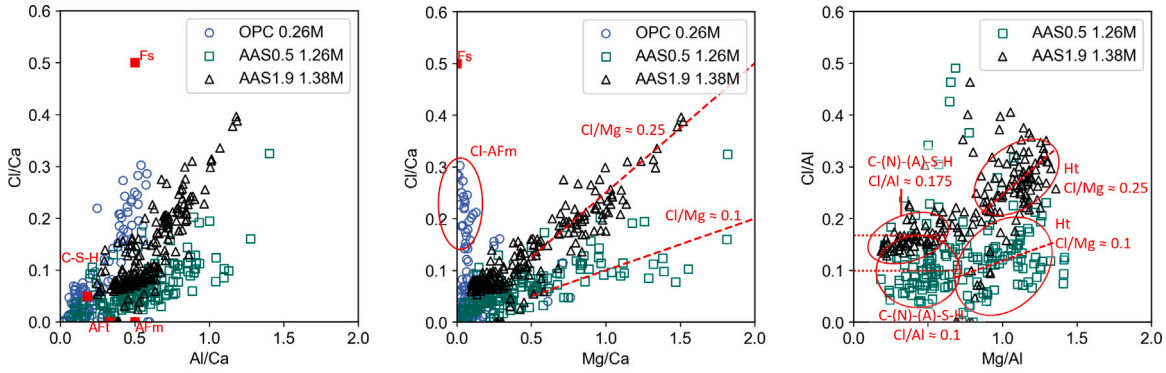

(a) (b) (c)

Fig. 15. SEM–EDS point analyses of polished samples of with 750× magnification.

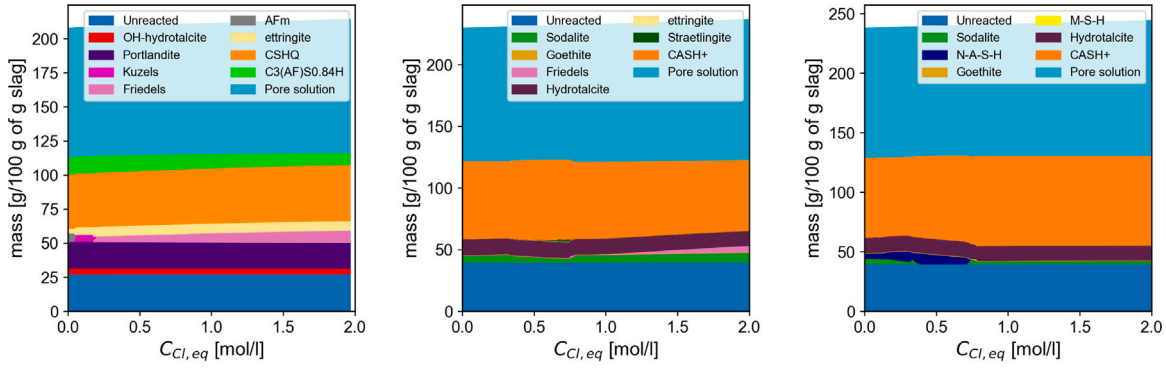

(a) OPC (b) AAS0.5 (c) AAS1.9

Fig. 16. Phase composition with increasing NaCl concentration in the constant volume of added solution $C_{Cl,added}$ of the OPC paste (DoH = 70%) and AAS pastes (DoH = 60%).

The determination of the bound chloride content of AAS pastes gives inconclusive results. The TGA analysis indicates for all AAS samples the highest chloride binding capacity in the hydrotalcite content. However, TGA quantification is only a rough estimate for AAS pastes as hydrotalcite, AFm phase and Friedel's salt release water in the same temperature range (see Section 2.4). The thermodynamic prediction evaluated based on *GEMS* Eq. (12) assumes chloride binding only in Friedel's salt with the ideal composition (Cl/Al = 1.0), but the phase formation is very limited. Therefore, the lowest chloride binding capacity of the AAS pastes is found using *GEMS* Eq. (12). The *XRD+EDS* quantification

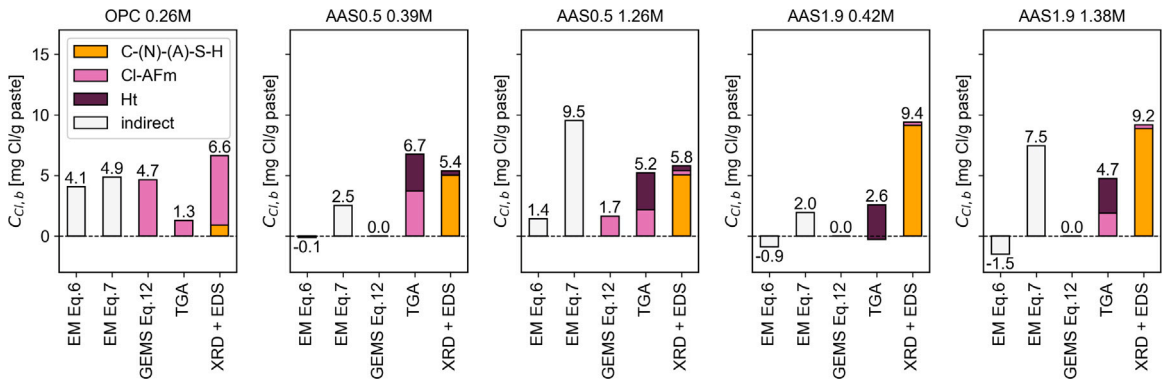

Fig. 17. Comparison of bound chloride content determined width different methods. Detailed description in Appendix A.8.

predicts limited binding in chloride-containing AFm phases and hydrotalcite based on the limited detection of this phases by Rietveld analysis. Due to the chloride binding in the C–(N)–(A)–S–H phase, the chloride binding in AAS1.9 paste is higher than in AAS0.5 paste, which contradicts the total chloride binding capacity determined based on the *equilibrium method* (*EM*). For AAS1.9 paste, the quantification with *XRD+EDS* also exceeds the indirect measurement based on the *equilibrium method*.

In summary, the direct measurement methods do neither confirm the indirect quantification of the chloride binding capacity using *equilibrium method* in combination with Eq. (6) nor Eq. (7). Furthermore, the AAS pastes give more inconclusive results compared to the OPC paste. The influence of the different evaluation methods of the *equilibrium method* (given in Table 3) will therefore discussed in detail in the following.

4.2. Neglecting initial water content

In this section the effects of neglecting initial water content in the *equilibrium method* evaluation is discussed. For this, the chloride binding capacity is evaluated indirectly by investigating the chloride concentration in the equilibrium solution ($C_{Cl,eq}$) and neglecting the initial water content ($m_{pore,0}$). Therefore, the evaluation protocol *EM* Eq. (7) (given in Table 3) is used to evaluate the *equilibrium method*, while for the evaluation of the thermodynamic prediction the prediction protocol *GEMS* Eq. (7) (given in Table 5) is used. The results are illustrated in Fig. 18(a).

For all pastes, $C_{Cl,b}$ from the *equilibrium method* agree well with $C_{Cl,b}$ derived from the equilibrium solution of the thermodynamic simulations, as illustrated in Fig. 18(a). The higher binding capacity based on the evaluation using *GEMS* Eq. (7) in Fig. 18(a), compared to the evaluation based on *GEMS* Eq. (12) given in Fig. 17, is caused by neglecting the initial water content of the paste. The added chloride concentration exceeds the initial concentration, leading to an artificially large difference relative to the equilibrium concentration and thus to an overestimation of chloride binding. This *diluting effect* becomes more pronounced at lower degrees of hydration, where larger pore solution volumes further reduce initial chloride concentration, and at higher concentrations of the added solution (see Appendix A.7). When $C_{Cl,init} \ll C_{Cl,add}$, the calculated chloride binding is dominated by dilution rather than by actual chloride binding.

Overall, the thermodynamic simulations in Fig. 18(a) confirm that neglecting the initial water content systematically overestimates chloride binding capacity due to the *diluting effect*. Given this systematic bias, the evaluation protocol *EM* Eq. (7) is not suitable for analysing chloride binding capacity of the *equilibrium method*. The alternative protocol *EM* Eq. (6) explicitly accounts for the initial water content, however the calculated negative binding capacity in this study violates mass conservation. The underlying assumptions and limitations of *EM* Eq. (6) are therefore discussed in the following.

4.3. Accounting for initial water content

In this section the chloride binding capacity is evaluated again indirectly by investigating $C_{Cl,eq}$ for both, thermodynamic modelling and the *equilibrium method*. To account for the initial water content, the evaluation protocol *EM* Eq. (6) to evaluate the *equilibrium method* and prediction protocol *GEMS* Eq. (6) to evaluate the thermodynamic prediction are applied. The results are illustrated in Fig. 18(b).

As illustrated in Fig. 18(b), the evaluation of $C_{Cl,b}$ yield similar trends for thermodynamic predictions and the *equilibrium method*. The AAS isotherms exhibit negative values of the chloride binding capacity, which is physically impossible as it violates mass conservation. This artefact arises from water-binding reactions occurring in the paste during equilibration. Thermodynamic modelling shows that the volume of the liquid phase decreases after equilibration for all binders, even when additional hydration of unreacted clinker is neglected (see Appendix A.7). While the total chloride mass in the system remains constant, the consumption of liquid volume leads to an increase in the equilibrium chloride concentration. In Eq. (6), which assumes a constant liquid volume, the difference between initial and equilibrium concentration is attributed entirely to chloride binding in the solid phase. Consequently, if equilibrium concentration is higher as the initial concentration, the calculated chloride binding capacity becomes negative.

When chloride binding is evaluated indirectly from the equilibrium solution, as in the *equilibrium method*, the calculated bound chloride content must therefore be corrected for changes in liquid volume to ensure mass conservation. This correction for the *volume effect* is illustrated in Fig. 19. The indirectly determined $C_{Cl,b}$ based on *GEMS* Eq. (6) corrected by $C_{Cl,Vol}$ equals the predicted chloride content in the Cl–AFm phases based on *GEMS* Eq. (12). The thermodynamic simulation confirms that the negative chloride binding capacity obtained using Eq. (6) arise exclusively from liquid volume reduction during equilibration. Correcting for this volume change fully resolves the negative binding.

For selected equilibrium samples the amount of chemically bound water was measured before and after exposure. Based on the difference in chemically bound water, the experimental determined bound chloride content based on *EM* Eq. (6) can also be corrected using $C_{Cl,vol}$ *Eq.* (8). For the AAS samples, this correction increases the calculated chloride binding capacity, as illustrated in Fig. 19. For AAS0.5 paste, the correction resolves the negative chloride binding and results a significant increase in binding capacity for the *AAS0.5 1.26M* sample. However, the negative binding capacity observed for AAS1.9 could not be compensated fully by this correction. It is possible that the degree of hydration (DoH) of the slag, and therefore the C–(N)–(A)–S–H content, in AAS1.9 paste increased more strongly during equilibration time than in the AAS0.5 paste. In this study, the chemically bound water content ($m_{H,chem}$) was determined based on solvent exchanged samples, which might leads to a underestimation of the increase of chemically bound water in the C–(N)–(A)–S–H phase.

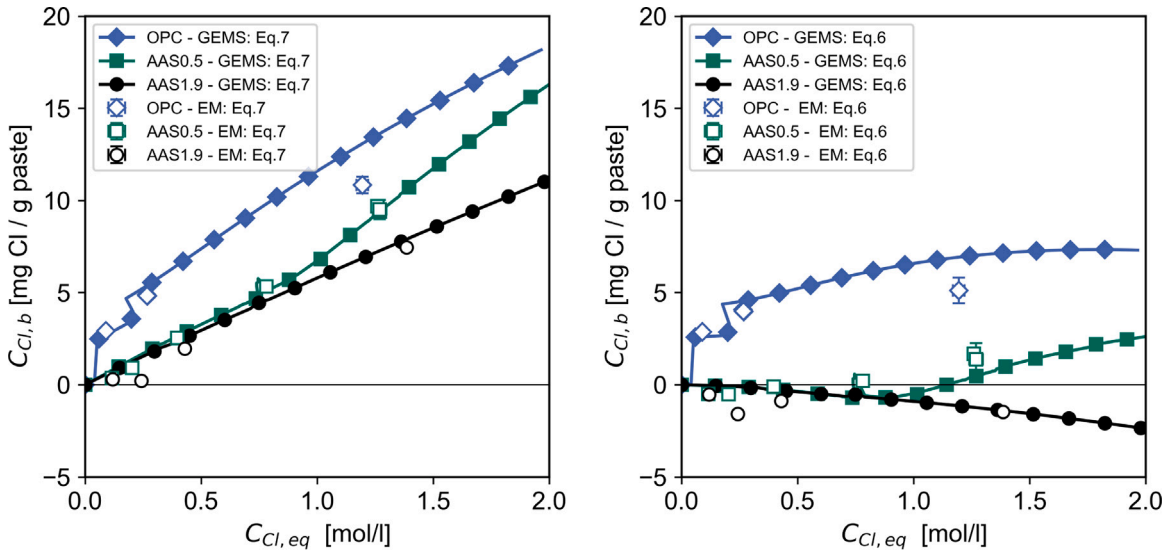

(a) Evaluation based on Eq. (7)

(b) Evaluation based on Eq. (6)

Fig. 18. Isotherms from the *equilibrium method* (*EM*) evaluated with different evaluation protocols (given in Table 3) and compared with thermodynamic prediction (*GEMS*) evaluated indirectly using the pore solution based on corresponding prediction protocols (given in Table 5).

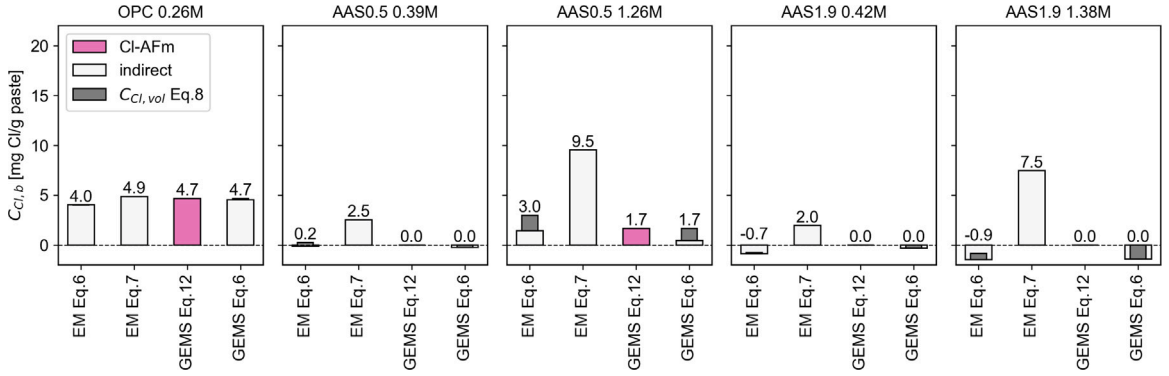

Fig. 19. Bound chloride content $C_{Cl,b}$ from the *equilibrium method* (EM) evaluated based on the evaluation protocol *EM* Eq. (6) corrected by Eq. (8) or based on *EM* Eq. (7) and, from the thermodynamic simulation evaluated based on the prediction protocols *GEMS* Eq. (12) or *GEMS* Eq. (6) corrected by Eq. (8).

4.4. Implications for chloride binding capacity of AAS

In this study, the experimental procedures and evaluation protocols of the *equilibrium method* used in six studies on AAS pastes [15,19,24,25,34,35] were analysed. All of these studies use evaluation protocols similar to *EM* Eq. (7) neglecting the initial water content, while only a subset [15,24,25,34] applied a drying step prior to exposure (see Appendix A.2). The results of the present study suggest that the comparatively high chloride binding capacities frequently reported for AAS pastes using the *equilibrium method* (see Fig. 7) may, at least in part, be attributed to dilution effects associated with the initial water content rather than to actual chloride binding. Consequently, the evaluation protocol *EM* Eq. (6) with the correction for the volume change of the liquid using Eq. (8) is recommended for AAS paste.

In this study negative chloride binding capacity of AAS pastes is observed during the equilibrium experiments with the evaluation protocol *EM* Eq. (6). Based on thermodynamic simulation it is demonstrated, that water binding reactions need to be compensated to be able to match the chloride binding capacity of the solid by indirect measurements of the equilibrium concentration. For AAS0.5, the correction based on the chemical bound water content full-fills the mass conservation requirement the experimental determination binding capacity as illustrated in Fig. 19. In contrast, for AAS1.9 the correction could not fully compensate the negative binding capacity, which might be due to reaction additional of previously unhydrated slag triggering a strong *volume effect*. Ongoing reactions in all AAS paste samples are indicated by several observations: (1) During the equilibrium experiments, increased agglomeration of the AAS paste grains was observed over time despite regular shaking. The AAS1.9 samples, which exhibited more negative chloride binding compared to AAS0.5, also showed the strongest agglomeration. (2) The amount of equilibrium solution that could be extracted from the equilibrium samples by centrifugation was significantly lower than for the OPC samples. (3) TGA indicates that the amount of C–(N)–(A)–S–H in the water exposed sample is higher compared to the sample prior exposure and XRD detects the formation of monosulfoaluminate phases in the equilibrium samples. (4) The chemically bound water content in the AAS equilibrium samples increased with increasing NaCl concentration.

In this study, we assume that changes in chemically bound water can directly represent the evolution of liquid volume. However, this

proposed correction of the liquid volume represents a simplification and may not fully capture the underlying physical processes. The bound water content was determined based on the mass loss in the range of 105–950 °C, which might include the mass loss due to the release of CO_2 from phases such as calcite. Furthermore, changes in the bound water content also occurs due to the incongruent dissolution of C–A–S–H gel resulting in leaching of the Al and Ca ions when exposed to chloride solutions. Wang et al. [68] and Jin et al. [69] have investigated the structural changes in the C–A–S–H gel exposed to chloride solution and observed decline in the Ca/Si and Al/Si ratios. This structural changes in the C–A–S–H gel, can also result in changes in the bound water for the gel phase ultimately affecting the measured chloride binding.

Although low chloride-binding capacities of AAS were measured using the *equilibrium method*, the SEM–EDS analysis confirmed chloride binding in the C–(N)–(A)–S–H phase, hydrotalcite and to a very limited amount in chloride-containing AFm phases. The SEM–EDS analysis of AAS pastes also revealed significant chemical changes of the C–(N)–(A)–S–H phase due to the exposure to water or NaCl solution after the equilibrium experiment, due to leaching of Na. This raises the question if equilibrium experiments generally need to be adjusted to prevent leaching, e.g. by adjusting the pH of the exposure solution as done in several studies [11,15,19,21,26,27,33,34]. Or if leaching in equilibrium experiments should be provoked since it also occurs in concrete structures exposed to NaCl solution [65].

5. Conclusions

This study critically evaluates experimental *equilibrium method* and its evaluation protocols for determining chloride binding isotherms in Ordinary Portland cement (OPC) and alkali-activated slag (AAS) systems. By systematically comparing different evaluation protocols for determining chloride binding, this work highlights critical pitfalls in both experimental methodology and data interpretation.

This study demonstrates, that for AAS pastes the identification and quantification of the chloride-binding phases Friedel's salt and hydrotalcite based on TGA and XRD is highly uncertain. To identify all chloride-binding phases, including the C–(N)–(A)–S–H phase, additional SEM–EDS measurements are needed. This study further demonstrates that, even for SEM–EDS measurements, sample preparation (e.g., grains, polishing, powdering) and measurement method (e.g., point analysis, mapping) can influence the detection of phases, especially when their volume fraction is limited. If thermodynamic data is available for the binder systems studied, thermodynamic modelling provides a powerful complementary tool for assessing whether the paste composition or the pore solution volume is expected to change during equilibrium experiments.

For the *equilibrium method* it is shown that neglecting the initial water content, a common simplification in previous studies, introduces a *diluting effect* that lowers the measured equilibrium chloride concentration and consequently leads to an overestimation of the bound chloride content. This is especially important for AAS binders, which exhibit the finer pore structure and can therefore contain higher moisture content at a given relative humidity.

Although accounting for the initial water content, physically impossible negative chloride binding capacities are identified for AAS pastes for the first time, revealing fundamental limitations in conventional evaluation procedures of the *equilibrium method*. This study demonstrates that volume changes by additional water binding reactions can substantially affect the indirectly determined binding capacity. Such water binding reactions are likely to occur for AAS pastes, because water-curing before exposure is not recommended for AAS pastes due to leaching issues. The novelty of this work lies in introducing a correction for this error of the *volume effect*, achieved for the first time by quantifying the chemically bound water content both before and after exposure.

As a conclusion from this study, practical recommendations to refine the *equilibrium method* are provided in the next section. The establishment of clear guidelines for the experimental procedure, for the evaluation protocol and for reporting essential parameters, aims to improve the reliability and comparability of chloride binding studies.

6. Recommendations for the *equilibrium method*

This study highlights, that the experimental procedure of the *equilibrium method* in combination with the applied evaluation protocol influences the reported chloride binding capacity. Especially for alternative binder systems, the chloride binding capacity is sensitive to the evaluation protocol used. When evaluating alternative binder systems, particular attention should be paid to the *diluting effect*, as it becomes more pronounced for binders with low chloride-binding capacity. In contrast, the *volume effect* should be taken into account for any binder that has the potential to react with the chloride-containing exposure solution. To get reliable chloride binding isotherms the following steps should be kept in mind:

- Before exposure, the paste needs to exhibit a high degree of hydration. Ongoing hydration reduces the water content in the equilibrium sample, which leads to an underestimation of the binding capacity. Therefore, sample pre-treatment and sample age at exposure should be reported.
- Using SEM–EDS, leaching of all pastes exposed to water or NaCl-solution was observed, altering the C–(N)–(A)–S–H composition of the paste. To prevent leaching, the composition of the added solution can be adapted, which should be reported.
- The exposure time needs to be long enough, so that equilibrium is reached. We recommend testing the reduction of the initial concentration $C_{Cl,init}$ [mol/l] during the experiment using additional equilibrium samples.
- During equilibration, water can become chemically bound, leading to an underestimation of the chloride binding capacity. The resulting error due to changes in liquid volume should be quantified using Eq. (8). The chemically bound water content should be determined before exposure and after equilibrium is reached. The chemically bound water content and the methodology applied for its determination should be reported.
- Drying of the samples before exposure to use Eq. (7) is not recommended, since the phase composition of the paste could be altered due to dehydration of phases such as C–(N)–(A)–S–H. On the other hand neglecting the initial water content leads to the *diluting effect*, which leads to a overestimation of the chloride binding capacity. Therefore, the determination of initial water content of the paste before exposure is recommended to use the evaluation protocol based on Eq. (6). The following parameters should be reported:
  - the chloride concentration of the added solution $C_{Cl,add}$ [mol/l], which should be experimentally confirmed,
  - the chloride concentration of the equilibrium solution $C_{Cl,eq}$ [mol/l],
  - the volume of the added concentration V_{added} [m^3], which should be limited to ensure detectable changes in the concentration and limit leaching,
  - the weight of the moist sample at exposure $m_{sample,0}$ [g] and,
  - the initial water content $m_{pore,0}$ [g], which can be determined e.g. by measuring the mass loss after 10 h at 40 °C in N_2 environment,
  - the chemically bound water content $m_{H,chem}$ before exposure and after equilibrium is reached e.g. by measuring the mass loss between 105 °C and 950 °C.

- To ensure that leakage did not occur, the sealed equilibriums samples (container, paste and liquid) should be weighted before exposure and after equilibrium was reached.
- When chloride binding isotherms are reported the x-axis should always be the concentration of the equilibrium solution $C_{Cl,eq}$ in [amount Cl/volume liquid]. The y-axis should be the bound chloride content at equilibrium $C_{Cl,b}$ in [amount Cl/ mass dry sample] and specific the dry state it refers to. This enables comparable results and helps to avoid unit conversion errors if used in reactive transport models.

CRediT authorship contribution statement

Annika Lidwina Schultheiß: Writing – original draft, Visualization, Validation, Software, Methodology, Investigation, Formal analysis, Data curation. **Klaartje de Weerdt:** Writing – review & editing, Supervision, Software, Methodology, Investigation, Funding acquisition, Formal analysis, Conceptualization. **Natalia Palina:** Writing – review & editing, Software, Investigation, Formal analysis. **Mayank Gupta:** Writing – review & editing, Software, Investigation, Formal analysis. **Barbara Lothenbach:** Writing – review & editing, Supervision, Methodology. **Ravi A. Patel:** Writing – review & editing, Supervision, Methodology, Conceptualization. **Frank Dehn:** Writing – review & editing, Supervision, Funding acquisition, Conceptualization.

Declaration of generative AI and AI-assisted technologies in the manuscript preparation process

During the preparation of this manuscript, the authors used ChatGPT (OpenAI) and DeepL (DeepL SE) for language refinement and text polishing, and GitHub Copilot (GitHub, Inc.) for assistance in creating figures and plots in Python. All generated content was critically reviewed, revised, and validated by the author(s), who take full responsibility for the integrity and accuracy of the final manuscript.

Declaration of competing interest

The authors declare that they have no known competing financial interests or personal relationships that could have appeared to influence the work reported in this paper.

Acknowledgements

Annika L. Schultheiß acknowledges financial support from the Karlsruhe House of Young Scientists (KHYS) for her research stay at NTNU. We thank Jostein Røstad (Thin Section Laboratory, Department of Geosciences, NTNU) for SEM–EDS sample preparation, Prof. Dr. Malene Thostrup Pedersen (Department of Structural Engineering, NTNU) for discussions on XRD analysis, and Kamila Zablocka Thostrup Pedersen (Department of Structural Engineering, NTNU) for discussions on titration and TGA.

Appendix A

A.1. Chloride binding prediction

Su et al. [10] present thermodynamically predicted chloride binding isotherms for OPC pastes blended with supplementary cementitious materials, which agree well with their experimental determined isotherms. However, the relatively short equilibration time of 48 h to determine the validation isotherms and the validation based on bound chloride per volume (instead of mass) of dry paste limits the reliability of their validation process.

Cao et al. [11] combined a thermodynamic model with a surface complexation model to predict chemical and physical chloride binding of OPC paste. However, the experimental validation isotherms

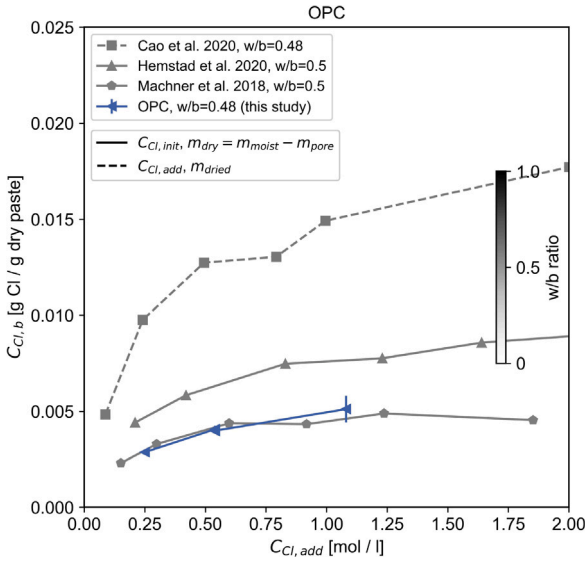

Fig. 20. Comparison the chloride binding capacity vs. the added chloride concentration $C_{Cl,added}$ of the OPC paste from this study with other OPC studies [11,13,30].

(measured at RH = 11%) yield binding capacities more than twice as high as those determined for comparable OPC pastes [13,30] as illustrated in Fig. 20. If the latter were applied as validation data, the predicted chemical binding determined by thermodynamic prediction alone is sufficient to match the observed binding. Hence, there is not the need to invoke additional physical binding on the basis of a surface complexation model.

A.2. Literature review

In Table 9, experimental procedures and evaluation protocols from previous studies using *equilibrium method* are summarized.

A.3. Mix design AAS paste

In Table 10, details of the chemical composition of the AAS paste and its activator are given.

A.4. TGA

The calculated phase amounts according to TGA is given in Table 11.

A.5. XRD

For the external standard, silicon is used as the standard, which was measured independently using the same method along with the other samples. For the diffractograms, the Rietveld analysis was performed using the Profex software. Initially using the standard material the instrument factor (K-factor) is calculated using the following equation

$$K = \frac{S_s \rho_s V_s^2 \mu_s}{W_s} \tag{13}$$

where S_s is the scale factor, ρ_s [g/cm^3] is the crystal density, V_s [cm^3] is the crystal volume of the unit cell, μ_s [cm^2/g] is MAC, and W_s is the weight fraction (calculated to be 100%) of the standard materials. μ_s can be calculated by referring the database on MAC values for each atom against the CuKα source. The XRD data for different samples were analysed using the Rietveld analysis. The phases used for the refinement are given in Table 12. Using the K factor calculated using

Table 9
Literature review of experimental procedure and evaluation protocol from studies using *equilibrium method* to determine chloride binding for OPC and AAS pastes.

Ref.	Binder	w/b	$n_{Cl,start}$	Age [days]	Sample prep.	Exposure sol.	Ref. mass	m_{pore} measurement	Eq. time [days]	solid/liquid	x-axis Iso.	y-axis Iso.
[26]	OPC	0.4–0.8	added	52	Immersed in lime sol., vacuum dried, stored at 11% RH.	NaCl + $Ca(OH)_2$	$m_{sample,dry}$	No	14	–	$C_{Cl,eq}$ [mol/l]	$C_{Cl,b}$ [mg/g dry paste]
[28]	OPC	0.45	added	>365	Immersed in lime sol., dried at 11% RH.	NaCl	$m_{sample,dry}$	No	21	–	$C_{Cl,eq}$ [mol/l]	$C_{Cl,b}$ [mg/g dry paste]
[27]	OPC	0.3, 0.5	added	>28	Sealed curing (2 to 9 month), 3 day vacuum drying, 1 month at 11% RH, 2 h vacuum.	NaCl and CH-saturated	$m_{sample,11RH} - m_{pore}$	In oven at 105 °C	180	?	$C_{Cl,eq}$ [mol/l]	$C_{Cl,b}$ [mg/g dry paste]
[32]	OPC+ SCMs	0.5	added	93	2 month sealed at 22 °C, 3 days vacuum dried, 1 month at 11% RH, crushed, 2 h vacuum.	NaCl	$m_{sample,11RH}$	No	120	0.25	$C_{Cl,eq}$ [mol/l]	$C_{Cl,b}$ [mg/g paste]
[33]	OPC+ SCMs	0.45	added	190	100 days at 95% RH, 3 month at 35% RH.	NaCl + 0.3 M KOH+ 0.05M NaOH (pH = 13.5)	$m_{sample,35RH}$	No	60	0.1	$C_{Cl,eq}$ [mol/l]	$C_{Cl,b}$ [mg/g paste]
[21]	OPC	0.53	added	>90	Water-curing, crushed.	NaCl + 0.1 M NaOH	?	No	60	–	$C_{Cl,eq}$ [mol/l]	$C_{Cl,b}$ [mol/kg binder]
[22,29]	OPC	0.4	init	>14	Sealed curing, crushed, moist sand (+30% water).	NaCl, $MgCl_2$ or, …	$m_{wet} - m_{pore}$	TGA 105 °C (N_2, 4 h)	60	2	$C_{Cl,eq}$ [mol/l]	$C_{Cl,b}$ [g/g cement] [22]; $C_{Cl,b}$ [g/g dry paste] [29]
[13]	OPC	0.5	init	224	Sealed curing, crushed, moist sand (+30% water).	NaCl/$CaCl_2$	$m_{wet} - m_{pore}$	TGA 40 °C until const.	30	2	$C_{Cl,add}$ [mol/l]	$C_{Cl,b}$ [g/g dry paste]
[11]	OPC	0.48	added	28	Stored 95% RH, dried 11% RH.	NaCl + $Ca(OH)_2$	$m_{sample,dry}$	No	60	–	$C_{Cl,add}$ [mol/l]	$C_{Cl,b}$ [mg/g dry paste]
[30]	OPC	0.5	init	217	Sealed curing, crushed, moist sand (+40% water).	NaCl/$CaCl_2$	$m_{wet} - m_{pore}$	Dried 40 °C 10 h	90	0.75	$C_{Cl,eq}$ [mol/l]	$C_{Cl,b}$ [g/g dry paste]
[31]	OPC	0.45	init	217	Sealed curing, crushed, moist sand (+35% water)	NaCl/$CaCl_2$	$m_{wet} - m_{pore}$	Vacuum oven 105 °C until const. mass.	45	0.4	$C_{Cl,eq}$ [mol/l]	$C_{Cl,b}$ [g/g dry paste]
[23]	OPC+ SCM	0.5	init	67	Stored 98% RH, crushed, moist sand (+30% water).	NaCl	m_{cement}	TGA 40 °C	60	2	$C_{Cl,add}$ [mol/l]	$C_{Cl,b}$ [g/g cement]
[10]	OPC+ SCM	0.5	?	35	Water cured, crushed, dried 50 °C, stored sealed.	NaCl	$m_{sample,0}$?	No	2	0.4	C_{Cl} [kg/m^3]	$C_{Cl,b}$ [kg/m^3 dry paste]
[15]	OPC/ AAS	0.5	added	38	Sealed curing, crushed, vacuum dried, 11% RH.	NaCl + 1M NaOH	$m_{dry} - m_{pore}$	?	60	0.31	$C_{Cl,eq}$ [mol/l]	$C_{Cl,b}$ [mg/g dry paste]
[24]	AAS	0.48	added	?	Cured 95% RH, crushed, dried 50 °C until const. mass.	NaCl	$m_{sample,dry}$	No	30	0.2	$C_{Cl,add}$ [mol/l]	$C_{Cl,b}$ [mg/g dry paste]
[34]	AAS	var.	?	31	Cured, crushed (<74 μm), stored ethanol, dried 65 °C.	NaCl + NaOH	m_{dry}	No	14	0.075	–	$C_{Cl,b}$ [mg/g dry paste]
[25]	AAS	0.45	added	?	Cured 95% RH, crushed, dried at 50 °C for 48 h.	NaCl	m_{dry}	No	14/30	0.2	$C_{Cl,add}$ [mol/l]	$C_{Cl,b}$ [mg/g dry paste]
[19]	AAS	0.4	added	104/ 194	Stored 43% RH.	NaCl + NaOH	$m_{sample,0}$	No	21	0.25	$C_{Cl,eq}$ [mol/l]	$C_{Cl,b}$ [mg/g moist paste]?
[35]	AAS	0.35, 0.4, 0.45	added	>28	28 day in water at 22 °C, crushed, dried vacuum at 60 °C for ≥72 h, ground, sieved, sealed stored.	NaCl, $CaCl_2$ or, $MgCl_2$	$m_{sample,0}$	No	30	0.125	$C_{Cl,eq}$ [mol/l]	$C_{Cl,b}$ [mg/g “dry” paste]

Table 10
Chemical composition GGBFS and alkaline solution for of AAS0.5 and AAS1.9 paste based on 100 g GGBFS.

	Total mass [g]	CaO [g]	SiO_2 [g]	Al_2O_3 [g]	Fe_2O_3 [g]	MgO [g]	K_2O [g]	Na_2O [g]	TiO_2 [g]	P_2O_5 [g]	MnO [g]	NaOH [g]	SO_3 [g]	H_2O [g]	Na_2O_{eq} [g]
GGBFS	100.0	38.8	36.3	12.8	0.6	8.0	0.6	0.3	1.0	0.0	0.3	0.0	0.2	0.0	0.0
Solution for AAS0.5	53.9	0.0	1.9	0.0	0.0	0.0	0.0	0.6	0.0	0.0	0.0	4.4	0.0	47.0	4.0
Solution for AAS1.9	58.9	0.0	7.4	0.0	0.0	0.0	0.0	2.2	0.0	0.0	0.0	2.3	0.0	47.0	4.0

Table 11
Phase mass m_{phase} [g phase/g sample] of Friedel's salt and hydrotalcite calculated from TGA based on Eqs. (9) and (10).

Phase	Equation	OPC 0.0	OPC 0.26M	AAS0.5 0.0M	AAS0.5 0.39M	AAS0.5 1.26M	AAS1.9 0.0M	AAS1.9 0.42M	AAS1.9 1.38M
Hydrotalcite	Eq. (9)	0.26	0.27	0.19	0.21	0.20	0.18	0.18	0.19
Friedel's salt	Eq. (10)	0.00	0.01	0.00	0.03	0.02	0.00	0.00	0.01

Table 12
Phase assemblage determined by XRD/Rietveld refinement for solvent-exchanged OPC, AAS0.5, and AAS1.9 samples. Values are given in wt.%. Corresponding PDF/ICSD reference files used for refinement are listed.

Phase	PDF/ICSD	OPC		AAS0.5			AAS1.9		
		0.0 M	0.26 M	0.0 M	0.39 M	1.26 M	0.0 M	0.42 M	1.38 M
Hydrotalcite	04-015-4253	–	–	1.22	1.36	1.35	–	–	–
Sulfoaluminate16[a]	01-083-1289	–	–	0.36	0.50	–	0.34	0.04	1.25
Friedel's salt	01-078-1219	–	8.50	–	0.74	0.97	–	0.11	0.74
C_3S (Alite)	ICSD 162744	11.26	10.01	–	–	–	–	–	–
C_2S (Belite)	00-049-1673	7.03	6.97	–	–	–	–	–	–
C_4AF (Ferrite)	01-074-3675	6.11	4.59	–	–	–	–	–	–
Ettringite	04-022-3982	6.52	8.26	–	–	–	–	–	–
Hemicarbonate	04-018-9908	7.71	2.50	–	–	–	–	–	–
Monocarbonate	01-087-0493	5.78	2.52	–	–	–	–	–	–
Portlandite	00-004-0733	22.33	23.64	–	–	–	–	–	–
Quartz	ICSD 174	0.66	0.48	–	–	–	–	–	–
Periclase (MgO)	01-071-1176	1.34	1.69	–	–	–	–	–	–
Amorphous	–	31.26	30.83	98.42	97.41	97.68	99.66	99.85	98.01

[a] Comment: lattice parameter C = [2.95–3.9].

the Eq. (13), the weight fraction of different crystalline phases were calculated using

$$W_i = \frac{S_i \rho_i V_i^2 \mu_p}{G} \tag{14}$$

where S_i is the scale factor, ρ_i is the crystal density, and V_i is the crystal volume of mineral phase i. μ_p [cm^2/g] denotes the MAC of the samples, and was calculated for each sample using

$$\mu_p = \frac{\mu_{paste} + m_{H_2O} \cdot \mu_{H_2O}}{1 + m_{H_2O}} \tag{15}$$

where μ_{paste} denote the MAC value for the paste sample calculated from the chemical composition given in Table 1. m_{H_2O} is the amount of H_2O estimated from the TGA analysis by calculating the mass loss up to 550 °C and μ_{H_2O} is the MAC value for the H_2O. While the weight fraction of the amorphous phase is estimated by subtracting the total weight fractions of the crystalline phases from unity, as given below:

$$W_{amor} = 1 - \sum W_i \tag{16}$$

The determined phase are given in Table 12.

A.6. SEM-EDS

Fig. 21 shows the SEM–EDS images of polished samples before exposure and after exposure to water. In Figs. 22 and 23, an analysis of the elemental ratios obtained from SEM–EDS point analysis is presented for the identification of the paste phases.

In the *supplementary material*, additional SEM–EDS measurements on the paste grains, which were powdered and pressed to pellets are given. In the chloride-exposed samples traces of Cl-containing AFm phases were identified by large area mapping. However, spatial information of the phase in the grain is lost due to the sample preparation method.

A.7. Thermodynamic prediction

In this study the Friedel's salt composition $Ca_2Al(OH)_6(Cl_2OH) \cdot 2H_2O$ was used for thermodynamic predictions. Reported thermodynamic properties of Friedel's salt summarized in Table 13 vary, which influences predicted amount of Friedel's salt. Some difference in the Standard Gibbs free energy of formation ($\Delta_f G°$), enthalpy of formation ($\Delta_f H°$) and entropy ($S°$) have been observed, indicating that the Friedel's salt amount depend on the chosen thermodynamic dataset, introducing uncertainty into the results (see Figs. 24–26).

A.8. Chloride quantification

The chloride content per paste $C_{Cl,b}$ [g Cl/g paste] can be calculates based on the sum of all chloride containing phases:

$$C_{Cl,b} = \sum_{phase} Cl_{phase} \cdot M_{Cl} \cdot \frac{m_{phase}}{M_{phase}} \tag{17}$$

where m_{phase} [g phase/g paste] mass fraction of phase, which can be determined by Rietveld analysis (Table 12), TGA quantification (Table 11) or, thermodynamic prediction, Cl_{phase} [mol Cl/mol phase] are the chloride content of the phase and, M_{phase} and M_{Cl} [g/mol] is the molar mass of the phase and of chloride.

For *XRD+EDS* quantification method, the C–(N)–(A)–S–H phase $M_{C-(N)-(A)-S-H}$ is estimated based on two attached hydroxyl groups and $m_{C-(N)-(A)-S-H}$ of the AAS pastes ($DoH = 0.6$) is determine from the Rietveld analysis (given in Table 12) as follows:

$$m_{C-(N)-(A)-S-H} = m_{Amorphous} - (1 - DoH) \tag{18}$$

Note, that the chloride content of the phase Cl_{phase} from EDS analysis is base on the analysis of one sample of a certain equilibrium chloride concentration. In reality Cl_{phase} should be described with a chloride binding isotherm, i.e. as a function of the concentration in the equilibrium solution. The input parameter used for the quantification of the chloride binding capacity in Fig. 17 are given in Table 14.

Appendix B. Supplementary material

Supplementary material related to this article can be found online at https://doi.org/10.1016/j.cemconres.2026.108373.

Data availability

Data will be made available on request.

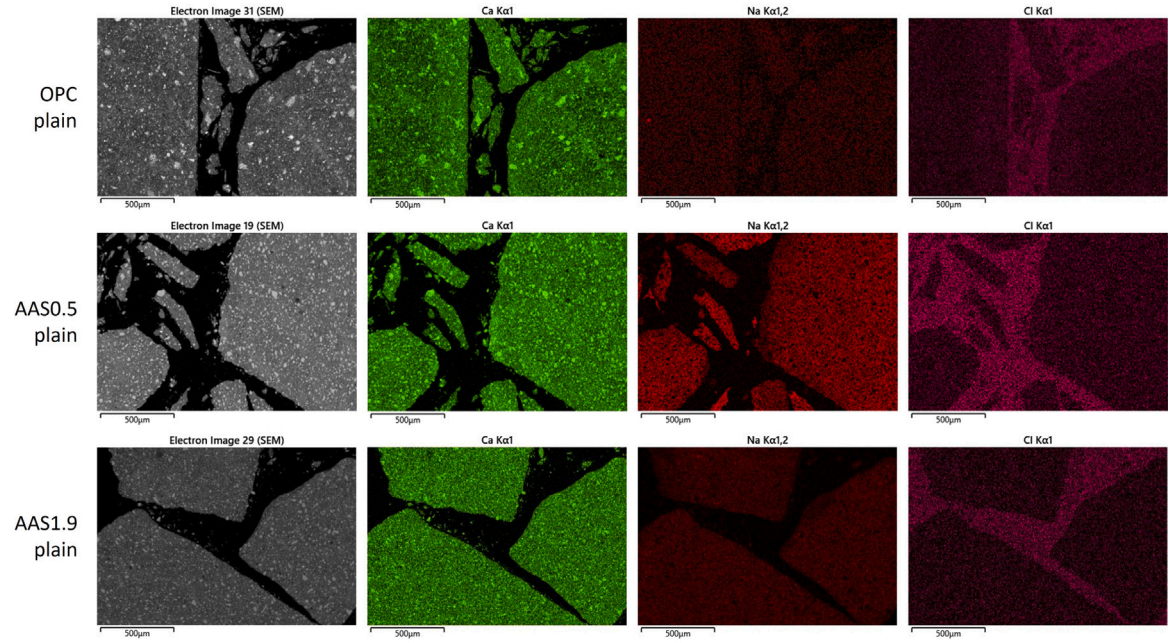

(a) plain

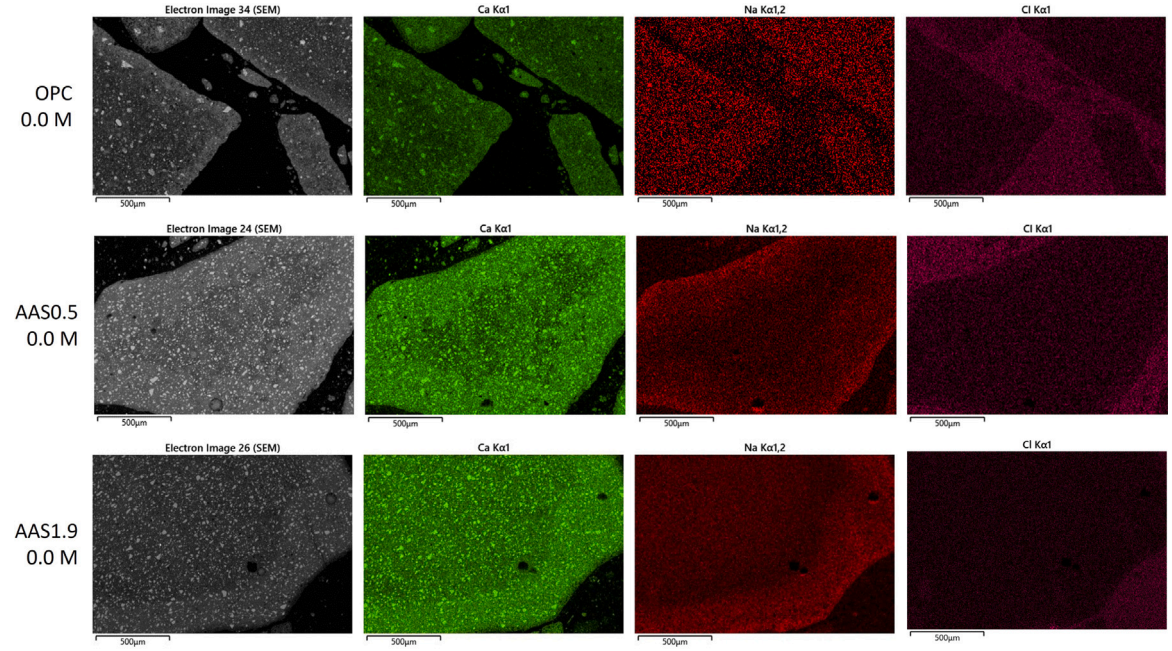

(b) 0.0 M

Fig. 21. Polished section of OPC, AAS0.5 and AAS1.9 samples at 75× magnification (a) before exposure measured with SEM–EDS and, (b) exposed to water.

Table 13
Thermodynamic properties of Friedel's salt from literature.

Ref	Chemical composition	$\Delta_f G^o$ [kJ/mol]	$\Delta_f H^o$ [kJ/mol]	S^o [J/mol K]
[48,70][a]	$Ca_4Al(OH)_{12}(Cl_2OH)\cdot 4H_2O$	−6810.9	−7604	731
[12]	$Ca_4Al_2(OH)_{12.05}Cl_{1.95}\cdot 4H_2O$	−6814.6	−7625	731
[71]	$Ca_4Al_2(OH)_{12}Cl_2\cdot 4H_2O$	−6815.44	−7670.04	527.7
[72]	$Ca_4Al_2(OH)_{12}Cl_{1.8}(CO_3)_{0.1}\cdot 4H_2O$	−6800 to −6860	–	680

[a] Used in this study.

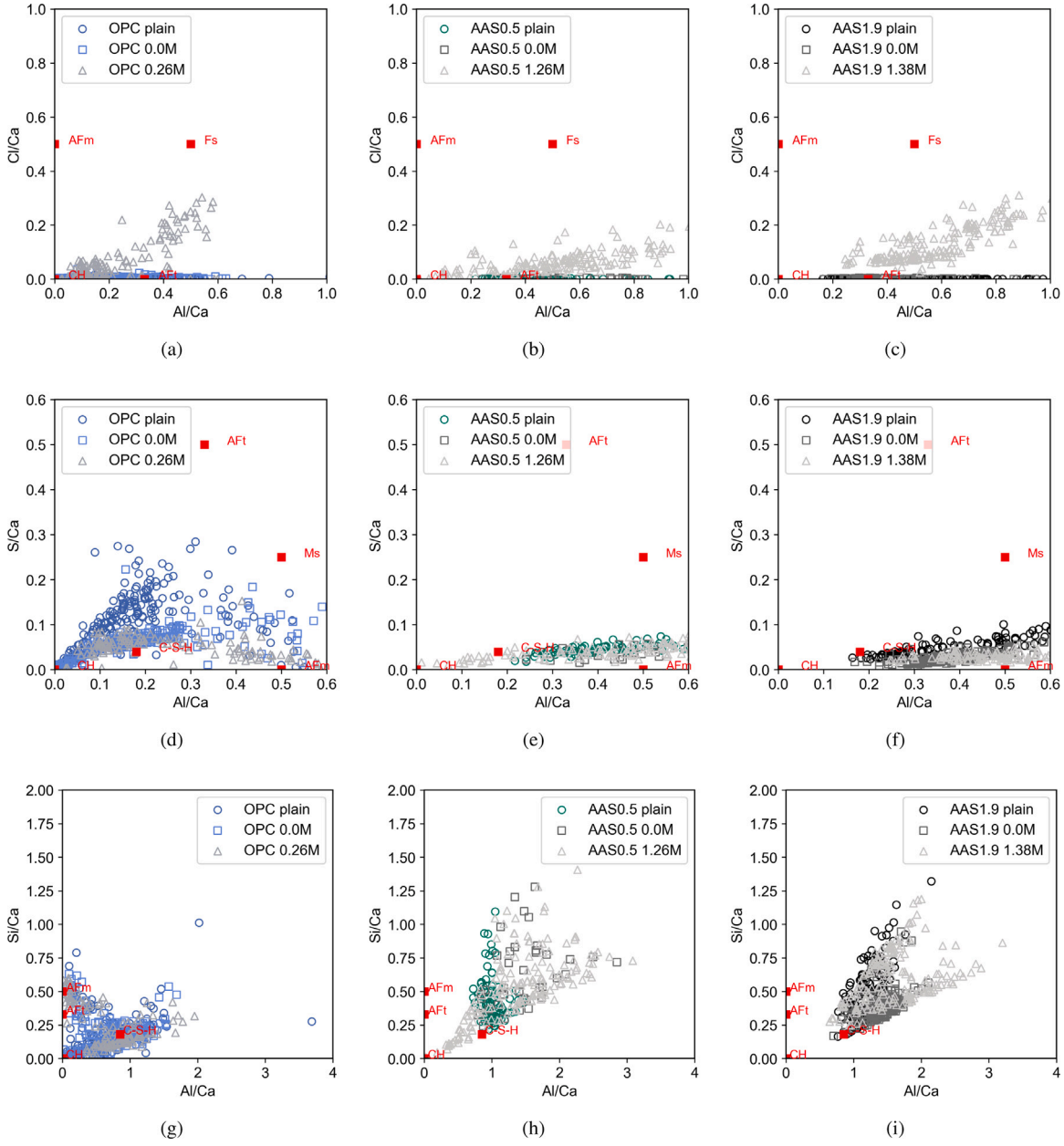

Fig. 22. SEM–EDS point analysis to characterize phase composition of the pastes.

Table 14
Input parameter used for the quantification of the chloride binding capacity for different methods.

Method	Phase	Chemical composition	M_{phase} [g/mol]	Cl_{phase} [mol Cl/mol phase]	Cl/Al	Cl/Mg	Reference
XRD+EDS	C-S-H (OPC)	$Ca_2Al_{0.3}Si_2 \cdot 2H_2O$	180.45	0.015	0.05	0	EDS analysis
	C-(N)-(A)-S-H (AAS0.5)	$Ca_{4.5}Na_{1.3}AlSi_{4.71} \cdot 2H_2O$	405.54	0.100	0.100	0	EDS analysis
	C-(N)-(A)-S-H (AAS1.9)	$Ca_{4.5}Na_{1.3}AlSi_{4.71} \cdot 2H_2O$	405.54	0.175	0.175	0	EDS analysis
	Hydrotalcite (AAS0.5)	$Mg_{5.4}Al_3(OH)_{18}(CO_3)_{1.5} \cdot 4.5H_2O$[a]	689.4	0.54[a]		0.10[a]	PDF 04-015-4253[a]
	Hydrotalcite (AAS1.9)	$Mg_{5.4}Al_3(OH)_{18}(CO_3)_{1.5} \cdot 4.5H_2O$[a]	689.4	1.35[a]		0.25[a]	PDF 04-015-4253[a]
	Cl-containing AFm (OPC)	$Ca_4Al_2(OH)_{12}Cl \cdot 4H_2O$[a]	525.8[a]	1[a]	0.5[a]		[48][a]
	Cl-containing AFm (AAS0.5)	$Ca_4Al_2(OH)_{12}Cl_{0.74} \cdot 4H_2O$[a]	516.6[a]	0.74[a]	0.37[a]		[48][a]
	Cl-containing AFm (AAS1.9)	$Ca_4Al_2(OH)_{12}Cl_{0.46} \cdot 4H_2O$[a]	506.7[a]	0.46[a]	0.23[a]		[48][a]
TGA	Friedel's salt	$Ca_4Al_2(OH)_{12}Cl_2 \cdot 4H_2O$	561.3	2	1		[48]
	Hydrotalcite	$Mg_4Al \cdot 10H_2O$	443.1	0.2			[16]
GEMS	Friedel's salt	$Ca_4Al_2(OH)_{12}Cl_2 \cdot 4H_2O$	561.3	2	1		[48]

[a] Adjusted based composition measured by SEM–EDS.

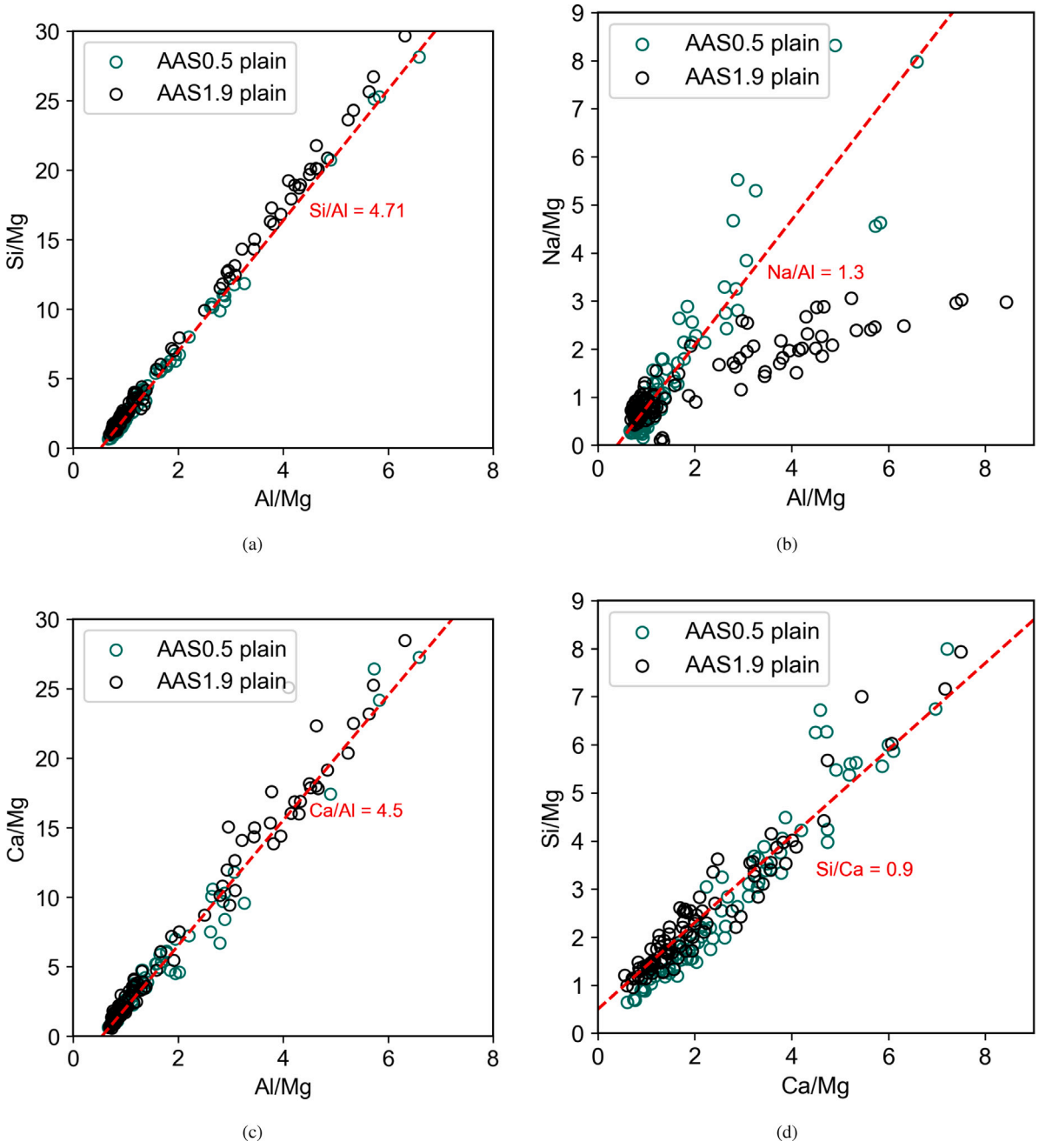

Fig. 23. SEM–EDS point analysis to characterize C–(N)–(A)–S–H phase.

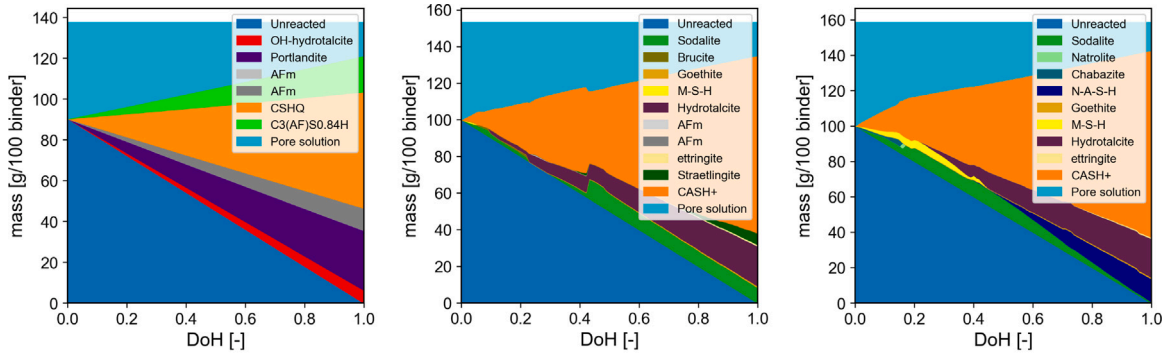

(a) OPC (b) AAS0.5 (c) AAS1.9

Fig. 24. Thermodynamic predicted development of the phase composition of the paste for increasing degree of hydration (DoH) of the OPC or slag.

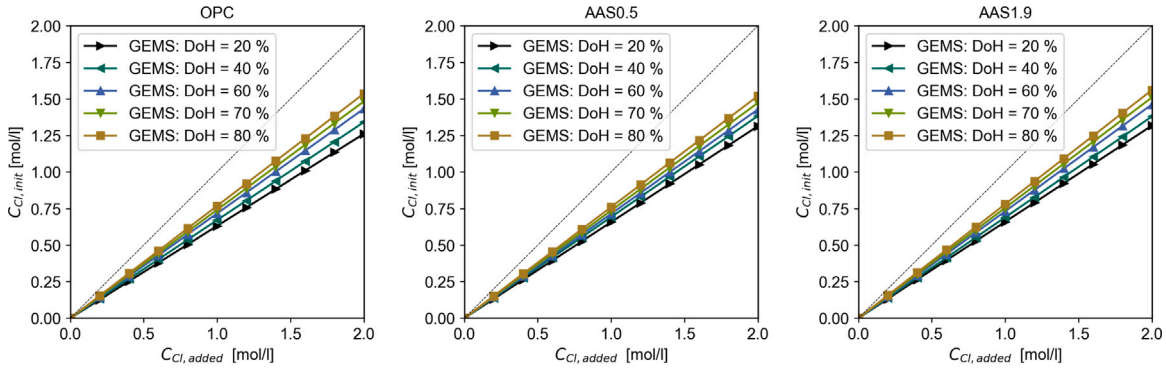

(a) OPC (b) AAS0.5 (c) AAS1.9

Fig. 25. Comparison of C_{init} with $C_{Cl,added}$ from thermodynamic prediction.

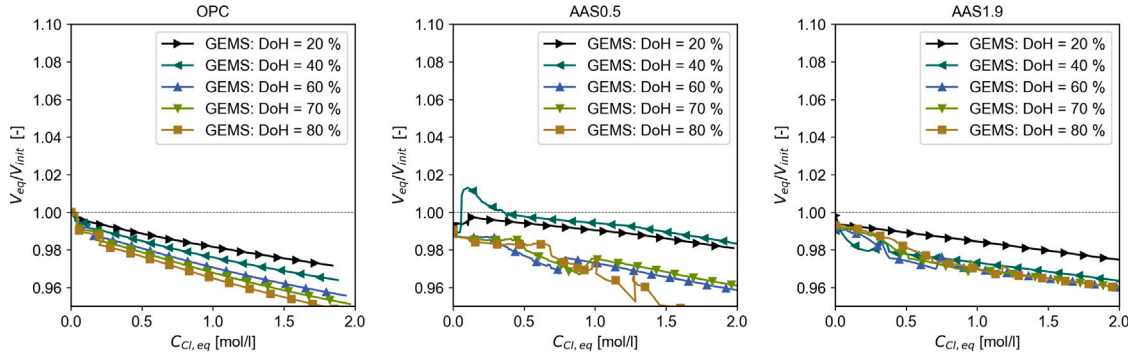

(a) OPC (b) AAS0.5 (c) AAS1.9

Fig. 26. Decrease of liquid volume during equilibrium experiment V_{eq} compared to the initial liquid volume V_{init} for different degree of hydration (DoH).

References

[1] Ueli M. Angst, Challenges and opportunities in corrosion of steel in concrete, Matér. Constr. 51 (1) (2018).

[2] Yao Ding, Jian-Guo Dai, Cai-Jun Shi, Mechanical properties of alkali-activated concrete: A state-of-the-art review, Constr. Build. Mater. 127 (2016) 68–79.

[3] Richard Caron, Ravi A. Patel, Frank Dehn, Experimental study on basic and drying creep for an alkali–activated slag concrete and comparison with existing creep models, Struct. Concr. (2023).

[4] Babatunde Abiodun Salami, Mohammed Ibrahim, Hassan Amer Algaifi, Wasiu Alimi, Adeoluwa Oladapo Ewebajo, A review on the durability performance of alkali-activated binders subjected to chloride-bearing environment, Constr. Build. Mater. 317 (2022) 125947.

[5] Julia T. Sonntag, Ravi A. Patel, David Alós Shepherd, Frank Dehn, Investigation of alkali-silica reaction on mortars with alternative binder systems: Alkali activated Slags and Celitement, Cement 13 (2023) 100078.

[6] Wenda Wu, Sixiang Kang, Xuefang Wang, Haojie Liu, Study on carbonation resistance and chloride ion distribution after carbonation of alkali-activated raw sea sand slag mortar, Case Stud. Constr. Mater. 19 (2023).

[7] DIN Deutsches Institut für Normung e. V., Zement - Teil 1: Zusammensetzung, anforderungen und konformitätskriterien von normalzement; deutsche fassung EN 197-1:2011, 2011.

[8] Neven Ukrainczyk, Thomas Bernard, Arezou Babaahmadi, Liming Huang, Christoph Zausinger, Anthony Soive, Stéphanie Bonnet, Fabien Georget, Maruša Mrak, Sabina Dolenec, Tobias Völker, Prannoy Suraneni, William Wilson, Test methods for chloride diffusivity of blended cement pastes: a review by RILEM TC 298-EBD, Matér. Constr. 58 (10) (2025).

[9] Fabien Georget, Arezou Babaahmadi, Alisa Machner, Maruša Mrak, Sabina Dolenec, Qing Xiang Xiong, Joseph Shiju, Didier Snoeck, Prannoy Suraneni, William Wilson, Measuring chloride binding in cementitious materials: A review by RILEM TC 298-EBD, Matér. Constr. 58 (10) (2025) 348.

[10] Peifeng Su, Qingli Dai, Evan S. Kane, Predicting chloride ingression in concrete containing different SCMs based on chloride binding and electrical resistivity, Constr. Build. Mater. 414 (2024) 134928.

[11] Yuanzhang Cao, Liping Guo, Bo Chen, Jiandong Wu, Thermodynamic modelling and experimental investigation on chloride binding in cement exposed to chloride and chloride-sulfate solution, Constr. Build. Mater. 246 (2020) 118398.

[12] Magdalena Balonis, Barbara Lothenbach, Gwenn Le Saout, Fredrik P. Glasser, Impact of chloride on the mineralogy of hydrated Portland cement systems, Cem. Concr. Res. 40 (7) (2010) 1009–1022.

[13] Alisa Machner, Maciej Zajac, Mohsen Ben Haha, Knut O. Kjellsen, Mette R. Geiker, Klaartje de Weerdt, Chloride-binding capacity of hydrotalcite in cement pastes containing dolomite and metakaolin, Cem. Concr. Res. 107 (2018) 163–181.

[14] J.J. Beaudoin, V.S. Ramachandran, R.F. Feldman, Interaction of chloride and C-S-H, Cem. Concr. Res. 20 (6) (1990) 875–883.

[15] Jian Zhang, Caijun Shi, Z. Zhang, Chloride binding of alkali-activated slag/fly ash cements, Constr. Build. Mater. 226 (2019) 21–31.

[16] Hailong Ye, Le Huang, Zhijian Chen, Influence of activator composition on the chloride binding capacity of alkali-activated slag, Cem. Concr. Compos. 104 (2019).

[17] Yong Zhang, Yuchi Fang, Ying Shen, Zhengxian Yang, Kai Wu, Chloride penetration and binding behavior in unsaturated alkali-activated slag mortars, Cem. Concr. Compos. 140 (2023).

[18] Xinyuan Ke, Susan A. Bernal, John L. Provis, Uptake of chloride and carbonate by Mg-Al and Ca-Al layered double hydroxides in simulated pore solutions of alkali-activated slag cement, Cem. Concr. Res. 100 (2017) 1–13.

[19] Gregor J.G. Gluth, Shishir Mundra, Ricky Henning, Chloride binding by layered double hydroxides (LDH/AFm phases) and alkali-activated slag pastes: an experimental study by RILEM TC 283-CAM, Matér. Constr. 57 (4) (2024) 1–17.

[20] Weixi Cai, Zhipeng Xu, Zhangmin Zhang, Jie Hu, Haoliang Huang, Yuwei Ma, Zuhua Zhang, Hao Wang, Suhong Yin, Jiangxiong Wei, Caijun Shi, Qijun Yu, Chloride binding behavior of synthesized reaction products in alkali-activated slag, Compos. Part B: Eng. 238 (2022) 109919.

[21] Mickael Saillio, Véronique Baroghel-Bouny, Fabien Barberon, Chloride binding in sound and carbonated cementitious materials with various types of binder, Constr. Build. Mater. 68 (2014) 82–91.

[22] K. de Weerdt, D. Orsáková, M.R. Geiker, The impact of sulphate and magnesium on chloride binding in Portland cement paste, Cem. Concr. Res. 65 (2014) 30–40.

[23] Zhenguo Shi, Mette Rica Geiker, Klaartje de Weerdt, Tone Anita Østnor, Barbara Lothenbach, Frank Winnefeld, Jørgen Skibsted, Role of calcium on chloride binding in hydrated Portland cement–metakaolin–limestone blends, Cem. Concr. Res. 95 (2017) 205–216.

[24] Tingli Yang, Xiaochun Fan, Xu Gao, Qian Gu, Shi Xu, Zhonghe Shui, Modification on the chloride binding capacity of alkali activated slag by applying calcium and aluminium containing phases, Constr. Build. Mater. 358 (2022).

[25] Xiaochun Fan, Yang Wang, Qingliang Yu, Xu Gao, Jiaolong Ye, Yu Zhang, Improving the chloride binding capacity of alkali activated slag by calcium and aluminum enriched minerals, J. Build. Eng. 70 (2023).

[26] Luping Tang, Lars-Olof Nilsson, Chloride binding capacity and binding isotherms of OPC pastes and mortars, Cem. Concr. Res. 23 (2) (1993) 247–253.

[27] Hassan Zibara, Binding of External Chlorides by Cement Pastes (dissertation), University of Toronto, Toronto, 2001.

[28] Anik Delagrave, Jacques Marchand, Jean-Pierre Ollivier, Simone Julien, Kati Hazrati, Chloride binding capacity of various hydrated cement paste systems, Adv. Cem. Based Mater. 6 (1) (1997) 28–35.

[29] K. de Weerdt, A. Colombo, L. Coppola, H. Justnes, M.R. Geiker, Impact of the associated cation on chloride binding of Portland cement paste, Cem. Concr. Res. 68 (2015) 196–202.

[30] Petter Hemstad, Alisa Machner, Klaartje de Weerdt, The effect of artificial leaching with HCl on chloride binding in ordinary Portland cement paste, Cem. Concr. Res. 130 (2020) 105976.

[31] Arezou Babaahmadi, Alisa Machner, Wolfgang Kunther, João Figueira, Petter Hemstad, Klaartje de Weerdt, Chloride binding in Portland composite cements containing metakaolin and silica fume, Cem. Concr. Res. 161 (2022) 106924.

[32] M.D.A. Thomas, R.D. Hooton, A. Scott, H. Zibara, The effect of supplementary cementitious materials on chloride binding in hardened cement paste, Cem. Concr. Res. 42 (1) (2012) 1–7.

[33] Andrej Ipavec, Tomaž Vuk, Roman Gabrovšek, Venčeslav Kaučič, Chloride binding into hydrated blended cements: The influence of limestone and alkalinity, Cem. Concr. Res. 48 (2013) 74–85.

[34] Yaguang Zhu, Xiaomei Wan, Xiao Han, Jie Ren, Juqian Luo, Qi Yu, Solidification of chloride ions in alkali-activated slag, Constr. Build. Mater. 320 (2022).

[35] Gaofeng Zhou, Wei Chen, Dazhi Wu, Keyu Chen, Peijun Tian, Meiling Chen, Influence of chloride salts on the chloride binding capacity of ab alkali-activated slag, Ceram. - Silik. 70 (1) (2026) 1–11.

[36] Karen Scrivener, Ruben Snellings, Barbara Lothenbach (Eds.), A Practical Guide to Microstructural Analysis of Cementitious Materials, first issued in paperback ed., CRC Press, Boca Raton and London and New York, 2017.

[37] Pamela Zuschlag, The Impact of Curing Temperatures on Portland Composite Cements – Hydrate Assemblage, Porosity, and Compressive Strength (Dissertation), Norwegian University of Science and Technology, Trondheim, October 2022.

[38] Frank Collins, J.G Sanjayan, Effect of pore size distribution on drying shrinking of alkali-activated slag concrete, Cem. Concr. Res. 30 (9) (2000) 1401–1406.

[39] Biao Wu, Xiaowen Chen, Dongwei Hou, Modeling of monolayer water adsorption on surface of cement minerals by molecule simulation and adsorption isotherm, Mater. Today Commun. 36 (2023) 106646.

[40] John L. Provis, Alkali-activated Binders and concretes: The path to standardization, in: Leslie Struble, James K. Hicks (Eds.), Geopolymer Binder Systems, ASTM International, 100 Barr Harbor Drive, PO Box C700, West Conshohocken, PA 19428-2959, 2013, pp. 185–195.

[41] Richard Caron, Ravi A. Patel, Frank Dehn, Extension of the fib MC 2010 for basic and drying shrinkage of alkali–activated slag concretes, Struct. Concr. (2022).

[42] Richard Caron, Ravi A. Patel, George D. Miron, Cassandre Le Galliard, Barbara Lothenbach, Frank Dehn, Microstructure development of slag activated with sodium silicate solution: Experimental characterization and thermodynamic modeling, J. Build. Eng. 71 (2023) 106398.

[43] Richard Caron, Ravi A. Patel, Frank Dehn, Activation kinetic model and mechanisms for alkali-activated slag cements, Constr. Build. Mater. 323 (2022) 126577.

[44] Alireza Dehghan, Karl Peterson, Graham Riehm, Lucas Herzog Bromerchenkel, Application of X-ray microfluorescence for the determination of chloride diffusion coefficients in concrete chloride penetration experiments, Constr. Build. Mater. 148 (2017) 85–95.

[45] Zhenguo Shi, Mette Rica Geiker, Barbara Lothenbach, Klaartje de Weerdt, Sergio Ferreiro Garzón, Kasper Enemark-Rasmussen, Jørgen Skibsted, Friedel's salt profiles from thermogravimetric analysis and thermodynamic modelling of Portland cement-based mortars exposed to sodium chloride solution, Cem. Concr. Compos. 78 (2017) 73–83.

[46] Chunyu Qiao, Prannoy Suraneni, Then Nathalene Wei Ying, Antara Choudhary, Jason Weiss, Chloride binding of cement pastes with fly ash exposed to CaCl2 solutions at 5 and 23 °C, Cem. Concr. Compos. 97 (2019) 43–53.

[47] Klaartje de Weerdt, Chloride binding in concrete: recent investigations and recognised knowledge gaps: RILEM Robert L'Hermite medal paper 2021, Matér. Constr. 54 (6) (2021).

[48] Barbara Lothenbach, Dmitrii A. Kulik, Thomas Matschei, Magdalena Balonis, Luis Baquerizo, Belay Dilnesa, George D. Miron, Rupert J. Myers, Cemdata18: A chemical thermodynamic database for hydrated Portland cements and alkali-activated materials, Cem. Concr. Res. 115 (2019) 472–506.

[49] Bin Ma, Barbara Lothenbach, Synthesis, characterization, and thermodynamic study of selected Na-based zeolites, Cem. Concr. Res. 135 (2020) 106111.

[50] Empa, Zeolite database 2021, 2025.

[51] Dmitrii A. Kulik, George Dan Miron, Barbara Lothenbach, A structurally-consistent CASH+ sublattice solid solution model for fully hydrated C-S-H phases: Thermodynamic basis, methods, and Ca-Si-H2O core sub-model, Cem. Concr. Res. 151 (2022) 106585.

[52] George Dan Miron, Dmitrii A. Kulik, Yiru Yan, Jan Tits, Barbara Lothenbach, Extensions of CASH+ thermodynamic solid solution model for the uptake of alkali metals and alkaline earth metals in C-S-H, Cem. Concr. Res. 152 (2022) 106667.

[53] Y. Yan, B. Ma, G.D. Miron, D.A. Kulik, K. Scrivener, B. Lothenbach, Al uptake in calcium silicate hydrate and the effect of alkali hydroxide, Cem. Concr. Res. 162 (2022) 106957.

[54] Kenneth S. Pitzer, Janice J. Kim, Thermodynamics of electrolytes. IV. Activity and osmotic coefficients for mixed electrolytes, J. Am. Chem. Soc. 96 (18) (1974) 5701–5707.

[55] H.C. Helgeson, D.H. Kirkham, G.C. Flowers, Theoretical prediction of the thermodynamic behavior of aqueous electrolytes by high pressures and temperatures; IV, calculation of activity coefficients, osmotic coefficients, and apparent molal and standard and relative partial molal properties to 600 degrees C and 5kb, Am. J. Sci. 281 (10) (1981) 1249–1516.

[56] Barbara Lothenbach, Gwenn Le Saout, Emmanuel Gallucci, Karen Scrivener, Influence of limestone on the hydration of Portland cements, Cem. Concr. Res. 38 (6) (2008) 848–860.

[57] J.J Chang, A study on the setting characteristics of sodium silicate-activated slag pastes, Cem. Concr. Res. 33 (7) (2003) 1005–1011.

[58] M. Ben Haha, B. Lothenbach, G. Le Saout, F. Winnefeld, Influence of slag chemistry on the hydration of alkali-activated blast-furnace slag — Part I: Effect of MgO, Cem. Concr. Res. 41 (9) (2011) 955–963.

[59] Gwenn Le Saoût, Mohsen Ben Haha, Frank Winnefeld, Barbara Lothenbach, Hydration degree of alkali–activated slags: A 29Si NMR study, J. Am. Ceram. Soc. 94 (12) (2011) 4541–4547.

[60] Susan A. Bernal, Rackel San Nicolas, Rupert J. Myers, Ruby Mejía de Gutiérrez, Francisca Puertas, Jannie S.J. van Deventer, John L. Provis, MgO content of slag controls phase evolution and structural changes induced by accelerated carbonation in alkali-activated binders, Cem. Concr. Res. 57 (2014) 33–43.

[61] Shiyu Sui, William Wilson, Fabien Georget, Hamed Maraghechi, Hadi Kazemi-Kamyab, Wei Sun, Karen Scrivener, Quantification methods for chloride binding in Portland cement and limestone systems, Cem. Concr. Res. 125 (2019) 105864.

[62] H. Poellmann, J. Neubauer, (Keine Angabe), Calcium aluminum oxide sulfate hydrate PDF 00-044-0602, 1993.

[63] Luis G. Baquerizo, Thomas Matschei, Karen L. Scrivener, Mahsa Saeidpour, Lars Wadsö, Hydration states of AFm cement phases, Cem. Concr. Res. 73 (2015) 143–157.
[64] M. Ben Haha, B. Lothenbach, G. Le Saout, F. Winnefeld, Influence of slag chemistry on the hydration of alkali-activated blast-furnace slag — Part II: Effect of Al2O3, Cem. Concr. Res. 42 (1) (2012) 74–83.
[65] Alisa Machner, Marie H. Bjørndal, Harald Justnes, Lucija Hanžič, Aljoša Šajna, Yushan Gu, Benoît Bary, Mohsen Ben Haha, Mette R. Geiker, Klaartje de Weerdt, Effect of leaching on the composition of hydration phases during chloride exposure of mortar, Cem. Concr. Res. 153 (2022) 106691.
[66] Satoshi Yoshida, Yogarajah Elakneswaran, Toyoharu Nawa, Electrostatic properties of C–S–H and C-A-S-H for predicting calcium and chloride adsorption, Cem. Concr. Compos. 121 (2021) 104109.
[67] Tiao Wang, Yuqian Zheng, Hao Qian, Zhenguo Shi, Satya MEDEPALLI, Jin Zhou, Fuqiang He, Tetsuya Ishida, Dongshuai Hou, Gaozhang Zhang, Zhengwu Jiang, Zhengning Zhou, Wei Zhang, Effects of Al in C–A–S–H gel on the chloride binding capacity of blended cement paste, Cem. Concr. Res. 190 (2025) 107805.
[68] Cun Wang, Binggen Zhan, Qijun Yu, Peng Gao, Binglin Guo, Lingling Zhu, Huyong Qin, Yuanhang Xu, Investigation on combined mechanical-chemical activation and its synergistic benefits for recycled concrete powder, J. Build. Eng. 117 (2026) 114870.
[69] Shucheng Jin, Kai Liu, Gaozhan Zhang, Hua Shi, Qingjun Ding, Wenyuan Xu, Effect of corrosive ions (Cl−, SO42−, and Mg2+) on the nanostructure and chloride binding property of C-A-S-H gel, J. Wuhan Univ. Technol.-Mater Sci. Ed. 35 (6) (2020) 1061–1072.
[70] Magdalena Balonis, Fredrik P. Glasser, Calcium nitrite corrosion inhibitor in Portland cement: Influence of nitrite on chloride binding and mineralogy, J. Am. Ceram. Soc. 94 (7) (2011) 2230–2241.
[71] Ph. Blanc, X. Bourbon, A. Lassin, E.C. Gaucher, Chemical model for cement-based materials: Thermodynamic data assessment for phases other than C–S–H, Cem. Concr. Res. 40 (9) (2010) 1360–1374.
[72] Roman O. Grishchenko, Anna L. Emelina, Pavel Y. Makarov, Thermodynamic properties and thermal behavior of Friedel's salt, Thermochimica Acta 570 (2013) 74–79.